Cell Reports

Article

A Bacteriophytochrome Mediates Interplay between Light Sensing and the Second Messenger Cyclic Di-GMP to Control Social Behavior and Virulence

Graphical Abstract

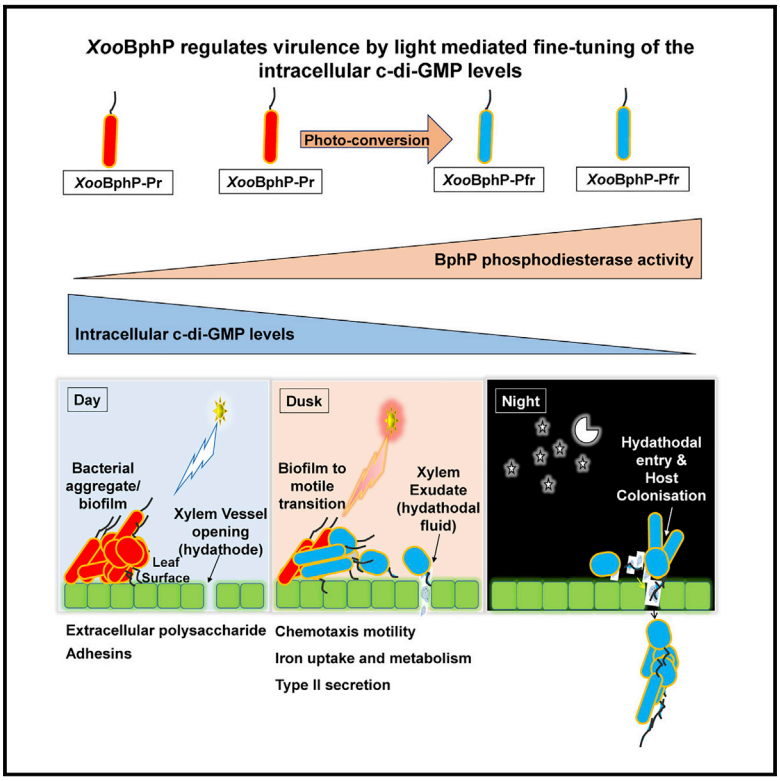

Highlights

- BphP is a bathy-type bacteriophytochrome involved in sensing light in *Xanthomonas*
- BphP degrades ubiquitous bacterial second messenger c-di-GMP in response to light
- BphP regulates virulence-associated functions in a light-dependent fashion
- Light-dependent modulation of c-di-GMP triggers sessile-to-motile transition

Authors

Raj Kumar Verma, Anindya Biswas, Akanksha Kakkar, Santosh Kumar Lomada, Binod Bihari Pradhan, Subhadeep Chatterjee

Correspondence

subhadeep@cdfd.org.in

In Brief

Verma et al. show that the bacterial photoreceptor BphP phytochrome is a light-sensing phosphodiesterase that modulates the intracellular secondary messenger cyclic di-GMP to regulate diverse social traits and virulence-associated functions in *Xanthomonas*. The light-dependent phosphodiesterase activity of BphP triggers changes in c-di-GMP and regulates virulence-associated functions.

Verma et al., 2020, Cell Reports *32*, 108202
September 29, 2020
https://doi.org/10.1016/j.celrep.2020.108202

CellPress

Cell Reports

CellPress
OPEN ACCESS

Article

A Bacteriophytochrome Mediates Interplay between Light Sensing and the Second Messenger Cyclic Di-GMP to Control Social Behavior and Virulence

Raj Kumar Verma,[1,2] Anindya Biswas,[1,2] Akanksha Kakkar,[1] Santosh Kumar Lomada,[1] Binod Bihari Pradhan,[1] and Subhadeep Chatterjee[1,3,*]

[1]Centre for DNA Fingerprinting and Diagnostics, Uppal, Hyderabad 500039, India
[2]These authors contributed equally
[3]Lead Contact
*Correspondence: subhadeep@cdfd.org.in
https://doi.org/10.1016/j.celrep.2020.108202

SUMMARY

Bacteriophytochromes are the most abundant and ubiquitous light-sensing receptors in bacteria and are involved in time-of-day behavior or responses. However, their biological and regulatory role in non-photosynthetic bacteria is poorly understood, and even less is known about how they regulate diverse cellular processes. Here, we show that a bacteriophytochrome (*Xoo*BphP) from the plant pathogen *Xanthomonas oryzae* pv. *oryzae* perceives light signals and transduces a signal through its EAL-mediated phosphodiesterase activity, modulating the intracellular level of the ubiquitous bacterial second messenger c-di-GMP. We discover that light-mediated fine-tuning of intracellular c-di-GMP levels by *Xoo*BphP regulates production of virulence functions, iron metabolism, and transition from a sessile to a free-swimming motile lifestyle, contributing to its colonization of the host and virulence. *Xoo*BphP thus plays a crucial role in integrating photo-sensing with intracellular signaling to control the pathogenic lifestyle and social behavior.

INTRODUCTION

Light is one of the most abundant environmental signals and is sensed by diverse forms of life. Organisms from all kingdoms of life have evolved light-sensing photoreceptors that enable them to respond to different wavelengths of light and coordinate various cellular processes (Chen et al., 2004; van der Horst et al., 2007; Kiang et al., 2007; Idnurm and Crosson, 2009; Beattie et al., 2018). The role of light-mediated signal transduction in regulation of several physiological processes, such as photosynthesis, light harvesting, phototactic movement, and pigment synthesis, is well known, particularly in plants and photosynthetic bacteria (Vierstra and Davis 2000; van der Horst et al., 2007; Beattie et al., 2018).

Bacteria can exploit light signals as an essential stimulus to facilitate lifestyle adaptation to changing environmental conditions. Interestingly, certain non-photosynthetic bacteria have also been reported to respond to distinct qualities of light that modulate various cellular responses, such as pigment biosynthesis, stress response, DNA repair, and host-pathogen interactions (Davis et al., 1999; Giraud et al., 2002, 2005; Jaubert et al., 2008; Barkovits et al., 2008; McGrane and Beattie, 2017). In the intracellular pathogen *Brucella abortus*, it has been shown that exposure to light can promote infection in macrophages (Swartz et al., 2007). Recent studies have shown that different wavelengths of visible light also act as essential signals for certain plant pathogens, such as *Pseudomonas syringae*, *Agrobacterium tumifaciens*, and *Xanthomonas campestris*, for motility, attachment, and virulence (Santamaría-Hernando et al., 2018; Oberpichler et al., 2008; Bonomi et al., 2016).

Bacteriophytochromes are the most abundant and ubiquitous light sensing photoreceptors in bacteria; however, the mechanism involved in regulating diverse cellular processes is poorly understood outside of some prominent model photosynthetic bacteria (Giraud et al., 2002; Vierstra and Davis 2000; Auldridge and Forest 2011). In general, bacteriophytochromes act as transducers of light by reversible photoconversion between a red-absorbing state (Pr) and a far-red-absorbing state (Pfr) in cells to produce the corresponding biological outputs. Typically, bacteriophytochromes possess N-terminal photo-sensory modules consisting of the PAS2-cyclic guanosine monophosphate (cGMP) phosphodiesterase/adenyl cyclase/FhlA (GAF)-phytochrome-associated (PHY) domain triad and a C-terminal output/effector histidine kinase-like domain or a domain of unknown function (Giraud et al., 2002; Vierstra and Davis 2000; Rockwell et al., 2006; Auldridge and Forest 2011). In the majority of the non-photosynthetic bacteria, very little is known about the mechanism by which bacteriophytochromes transduce photosensing to a downstream intracellular signal transduction cascade to coordinate diverse cellular processes and social behavior (Davis et al., 1999; van der Horst et al., 2007; Beattie et al., 2018).

Cyclic di-GMP is one of the most widespread intracellular secondary messengers in bacteria and has an important role in

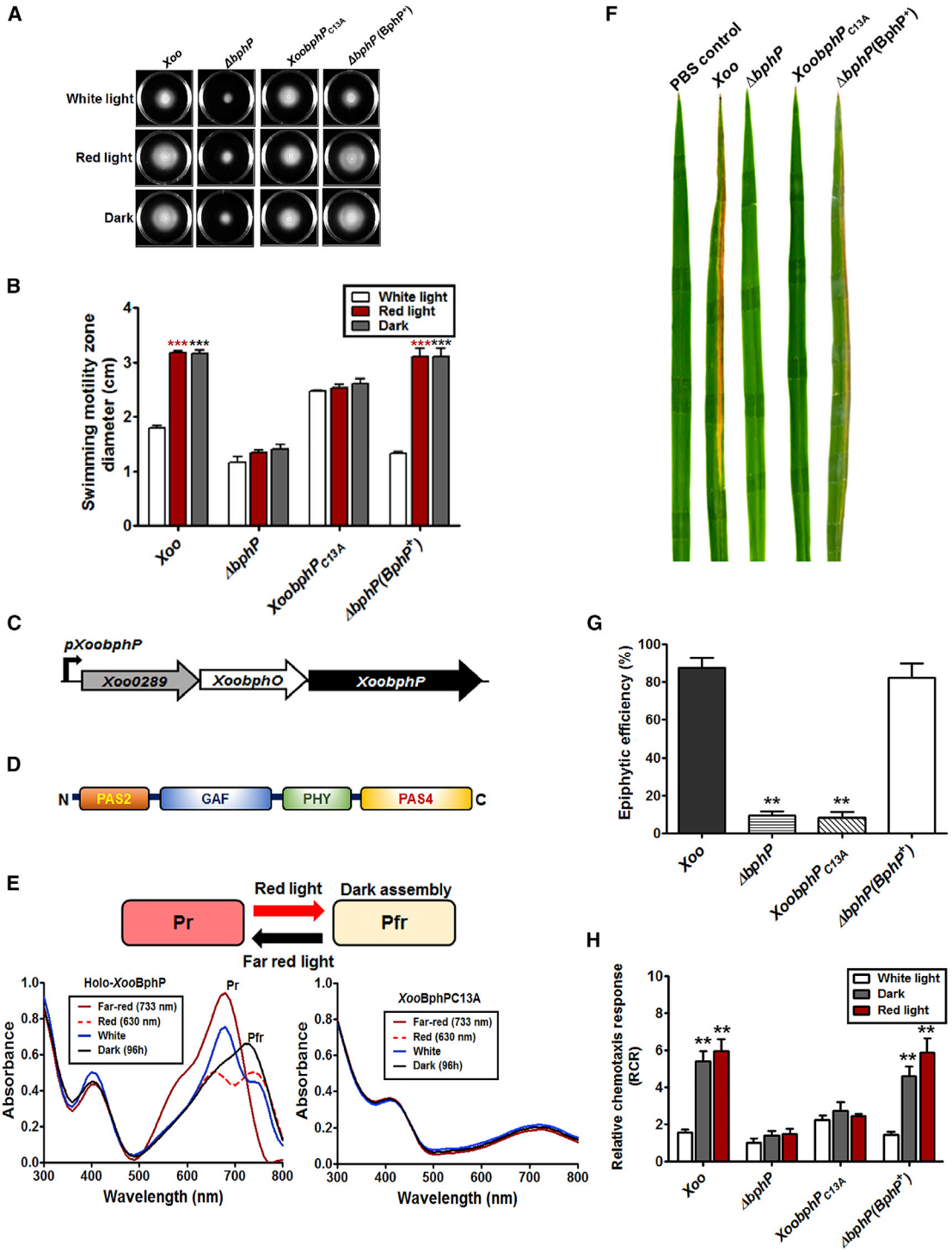

Figure 1. *Xoo*BphP Is a Bathy-type Bacteriophytochrome that Fine-Tunes the *Xoo* Natural Mode of Infection to Light

(A) Detection of swimming motility on semi-solid PS medium with 0.3% agar after cultivation for 3 days under different light conditions.

(B) Motility zone diameter quantification. Data are shown as the mean ± standard deviation (SD) (n = 3).

(C) Genomic organization of *Xoo*bphP.

(D) Domain architecture of *Xoo*BphP exhibiting an N-terminal photosensory module (PAS2-GAF-PHY triad) and C-terminal PAS4 domain.

(E) UV-vis absorption spectra of *Xoo*BphP and *Xoo*BphPC13A (light-insensitive variant) after dark adaptation and illumination with red, far-red, and white light. Pr and Pfr represent red-absorbing and far-red-absorbing, respectively.

(legend continued on next page)

regulation of gene expression by binding to RNA, various effectors, or regulatory proteins (Ryjenkov et al., 2005; Sondermann et al., 2012; Römling et al., 2013). In bacteria, fine-tuning of the intracellular level of c-di-GMP is maintained by its controlled and regulated synthesis and degradation, mediated by the enzymatic action of GGDEF- and EAL- or HD-GYP domain-containing proteins, respectively. It has been reported that the activity of c-di-GMP-modulating enzymes is regulated by various extracellular environmental signals and intracellular physiological conditions (Schirmer and Jenal 2009; Römling et al., 2013). Cellular c-di-GMP levels regulate various cellular and physiological processes, such as motility, biofilms, production of secreted and cell-associated virulence factors, cellular metabolism, and fine-tuning of the transition of a planktonic or free-living state to a multicellular aggregate or biofilm lifestyle (Ryjenkov et al., 2005; Jenal and Malone 2006; Römling and Simm 2009; Povolotsky and Hengge, 2012; Sondermann et al., 2012; Valentini and Filloux, 2016).

Xanthomonas oryzae pv. *oryzae* (*Xoo*), the causal agent of bacterial leaf blight disease of rice, is a vascular pathogen and an important member of the *Xanthomonas* group of phytopathogens, which causes severe disease in several economically important crops. During an epiphytic phase, *Xoo* forms biofilm-like structures to protect itself from hostile environmental stress on leaves subsequent to conditions in the plant after it enters the intercellular space through openings known as hydathodes, present at leaf tips, and eventually colonizes xylem vessels (Niño-Liu et al., 2006; Kumar Verma et al., 2018; An et al., 2020). Motility associated with switching between a biofilm lifestyle and a planktonic (motile) one has an important role in entry and subsequent colonization of the plant. Several virulence-associated functions, such as chemotaxis-driven motility, production of adhesins, expression of specialized iron uptake systems, cell-cell signaling, alteration of c-di-GMP levels, and production of various protein secretion systems, are required for *Xoo* infection of plants and its transition from a biofilm to a planktonic lifestyle. However, the environmental factors or cues that modulate this transition are still elusive (Dow, 2008; Büttner and Bonas, 2010; Bogdanove et al., 2011; Kumar Verma et al., 2018; An et al., 2020).

The *Xanthomonas* group of phytopathogens encodes a bacteriophytochrome, BphP, that has no predictable sensory output or effector domains that might be involved in downstream signal transduction (Otero et al., 2016). In this study, we show that the *Xoo* bacteriophytochrome (*Xoo*BphP) is a photosensing phosphodiesterase that specifically degrades c-di-GMP. *Xoo*BphP regulates motility, extracellular polysaccharide production, biofilm formation, and iron homeostasis by fine-tuning the intracellular levels of c-di-GMP in response to different wavelengths of light. This study provides mechanistic insights into the cascade of cellular changes following light perception by *Xoo*BphP and its modulation of the widely conserved second messenger signal to coordinate light-mediated regulation of social behavior important for its interaction with a host plant.

RESULTS

*Xoo*BphP Is a Cytosolic Bathy-type Bacteriophytochrome that Regulates Infection and Virulence in a Light-Dependent Fashion

In a swimming plate motility assay, wild-type (WT) *Xoo* exhibited reduced motility when exposed to white light compared with exposure to red light or in the dark (Figures 1A and 1B; Figures S1A and S1B). This prompted us to examine the role of light and light-mediated signaling in its virulence and social behavior.

Analysis of the *Xoo* genome revealed a gene encoding the putative bathy-type bacteriophytochrome BphP, *XoobphP* (*XOO0292*), which is located downstream of a gene encoding heme oxygenase (*XoobphO*) in a tri-cistronic operon (Figure 1C). Interrogation of this gene for conserved domains identifiable in protein family databases and multiple-sequence alignment analysis indicated that *Xoo*BphP has an N-terminal photo-sensing triad domain consisting of Per/Arndt/Sim (PAS2 family), GAF, PHY, and a PAS4 domain of unknown function (Figure 1D; Finn et al., 2014).

*Xoo*BphP has a conserved cysteine residue (Cys^{13}) (Figure S2B) that binds to Biliverdin-IXα (BV), an open-chain tetrapyrrole bilin chromophore, using the lyase activity of GAF, constituting holo-*Xoo*BphP (native form) (Davis et al., 2001; Auldridge and Forest, 2011; Otero et al., 2016).

To determine the *in vitro* functionality of *Xoo*BphP and to characterize its photo-sensing and spectral properties, we obtained recombinant N-terminal His-tagged *Xoo*BphP and its variant *Xoo*BphPC13A (Cys^{13} replaced with Ala) after expression in *E. coli* and purification (Figure S1D). The holo-protein was produced by incubating *Xoo*BphP with BV on ice for 1 h. Spectrophotometry experiments revealed that the holo-*Xoo*BphP is a bathy-type BphP because it exhibited Soret and Q bands (Abs_{400}/Abs_{750}) in the UV-visible (UV-vis) absorption spectra, indicative of a Pfr ground state and Pr-to-Pfr dark conversion (Otero et al., 2016). *Xoo*BphP exhibited a pure Pfr form after 96 h of dark adaptation (Figure 1E). Far-red irradiation (733 nm) promoted its photo-conversion to pure *Xoo*BphP-Pr, whereas red light irradiation (630 nm) promoted formation of a mixture of Pfr and Pr forms (Figure 1E). A similar result was obtained when dark-adapted *Xoo*BphP was irradiated with white light (Figure 1E). However, *Xoo*BphPC13A failed to exhibit light-induced photo-conversion (Figure 1E), suggesting that its chromophore is essential for its photo-conversion. We therefore used *Xoo*BphPC13A (a light-insensitive variant of *Xoo*BphP) as a control in all further studies.

To further characterize *Xoo*BphP and its cellular localization, we integrated a copy of C-terminally FLAG-tagged *XoobphP* under control of the endogenous promoter into the *XoobphP* genomic locus. The FLAG-tagged *Xoo* WT derivative exhibits a similar phenotype as the WT strain. Immunoblot analysis of different subcellular fractionations with an anti-FLAG antibody confirmed the cytoplasmic localization of *Xoo*BphP (Figure S1C).

(F and G) 21 dpi bacterial leaf blight (BLB) lesion of epiphytic infection by surface inoculation of Taichung Native-1' (TN-1) variety healthy leaves maintained under high humid conditions, and (G) determination of epiphytic efficiency after 21 days of surface inoculation. Data are shown as the mean ± SD (n = 20).
(H) Relative chemotaxis response (RCR) under different light conditions. Data are shown as the mean ± SD (n = 3).
Data shown in (B), (G), and (H): statistical significance by paired Student's t test (*$p < 0.05$, **$p < 0.01$, ***$p < 0.001$).

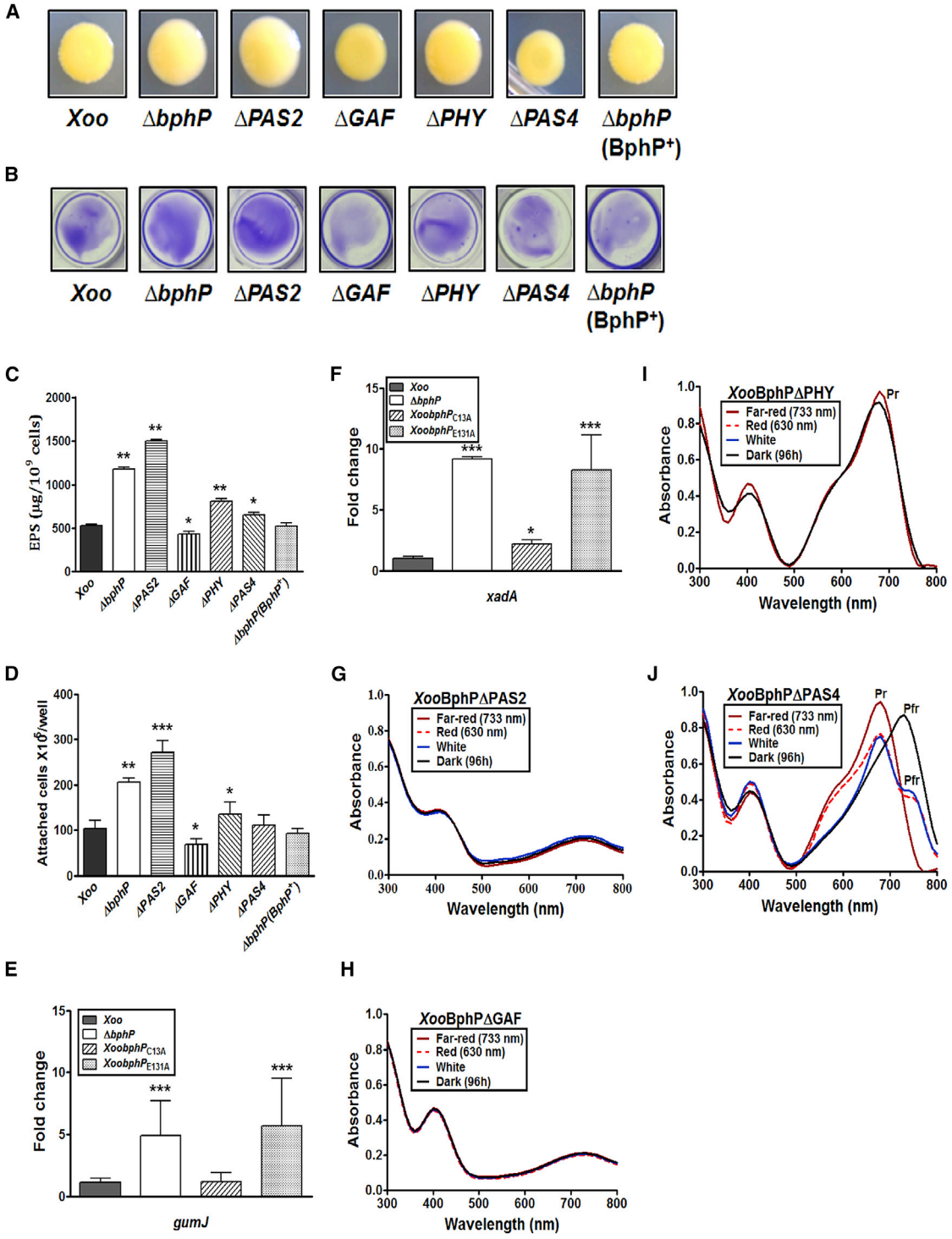

Figure 2. *Xoo*BphP Involves All Domains to Regulate the Virulence Program

(A) Extracellular polysaccharide (EPS) production in different strains of *Xoo*.

(B) Biofilm formation by strains of *Xoo* under static conditions after 48 h of growth.

(C) Quantification of EPS production by measuring absorbance at 214 nm, using D-glucose as a standard.

(D) Quantification of attached cells of *Xoo* strains in the static biofilm after 48 h of growth.

(legend continued on next page)

To understand the role of *Xoo*BphP *in vivo*, we constructed an in-frame deletion mutant of *XoobphP* (Δ*bphP*), and a light-insensitive point mutant, *XoobphP*$_{C13A}$ (the *Xoo* strain harboring the mutant *XoobphP*$_{C13A}$ allele in the *XoobphP* genomic locus). The Δ*bphP* mutant of *Xoo* did not exhibit any growth defect compared with *Xoo* in rich PS medium (Figure S1F). The WT or Δ*bphP*(BphP$^+$) (the Δ*bphP*-complemented strain harboring the WT *XoobphP* allele in the chromosome) exhibited significant increases in swimming motility under dark and red light compared with white light (*$p < 0.05$). In contrast, the Δ*bphP* and *XoobphP*$_{C13A}$ mutants exhibited reduced motility compared with the WT strain and did not differ in swimming motility under different light conditions (Figures 1A and 1B; $p > 0.05$). In contrast, white light promotes photo-conversion of Pfr to Pr forms (Figure 1E; Otero et al., 2016).

To determine the role of *Xoo*BphP-mediated light signaling in bacterial virulence, we assessed infection of plants from a topically applied inoculum where cells must enter the leaves through hydathodes (epiphytic infection or natural mode of infection; Kumar Verma et al., 2018; Pradhan et al., 2012; Rai et al., 2012). By 21 days after inoculation, Δ*bphP* and *XoobphP*$_{C13A}$ exhibited significantly reduced bacterial leaf blight (BLB) symptoms and epiphytic infection efficiency compared the WT *Xoo* strain or Δ*bphP*(BphP$^+$) (Figures 1F and 1G; Figure S1I). When directly inoculated into plant tissue by wounding, pre-exposed to darkness or red light conditions, the WT *Xoo* strain produced large lesions on leaves compared with those conferred by cells pre-exposed to white light. In contrast, *XoobphP*$_{C13A}$ exhibited reduced lesion size under all conditions, irrespective of the different light conditions to which it had been exposed (Figures S1G and S1H).

We next investigated whether the difference in infection seen in response to different light conditions was due to an altered chemotaxis response because flagellum-mediated motility and chemotaxis have important roles in entry and colonization of *Xoo* in rice leaves (Kumar Verma et al., 2018). We performed quantitative syringe capillary assays to measure the relative chemotactic response (RCR) of different strains of *Xoo* pre-exposed to darkness or red or white light to hydathodal fluid (xylem sap) collected from TN-1 rice leaves (Kumar Verma et al., 2018). The *Xoo* and Δ*bphP*(BphP$^+$) strains exhibited a significantly higher RCR when pre-exposed to darkness or red light than those exposed to white light. In contrast, Δ*bphP* and *XoobphP*$_{C13A}$ exhibited a lower RCR under all light conditions (Figure 1H). Furthermore, expression of various methyl-accepting chemotaxis receptor proteins (MCPs), essential for the chemotactic response in *Xoo* (Kumar Verma et al., 2018), by qRT-PCR revealed that these MCPs were downregulated in the Δ*bphP* and *XoobphP*$_{C13A}$ (Figure S2C) mutants compared with the WT strain.

Collectively, these data clearly indicate that *Xoo*BphP is an essential photoreceptor that regulates the infection process and virulence of *Xoo*.

*Xoo*BphP Regulates Several Virulence-Associated Functions, and Individual Domains Contribute

To investigate the role of the photosensor *Xoo*BphP itself and the essentiality of individual domains in regulation of virulence determinants, we focused on extracellular enzyme production (secreted by the T2SS; necessary for degradation of host cell wall components), motility (entry and colonization), xanthan gum production and EPS (extracellular polysaccharide; contributes to biofilm formation), siderophore production (sequestering iron in an iron-limited host environment) and the hypersensitive response (T3SS and its effectors to modulate virulence and host defense) (Büttner and Bonas, 2010; Bogdanove et al., 2011; Pandey et al., 2017; Kumar Verma et al., 2018; An et al., 2020).

We generated in-frame deletion mutants for each individual domain (Δ*PAS2*, Δ*GAF*, Δ*PHY*, and Δ*PAS4*) to determine their role in the abovementioned phenotypes (Figure S1D). The domain deletion mutants exhibited reduced virulence (Figures S3A and S3B), *in planta* migration defects (Figure S3C), and reduced motility (Figures S3E and S3G), similar to the full-length deletion mutant (Δ*bphP*). Measurement of the bacterial population in the rice leaves indicated that the Δ*bphP* mutant exhibited significantly reduced population sizes (~2.9 fold) compared with the WT *Xoo* strain at 7 dpi and 1.2-fold less than the WT strain at 12 dpi (Figure S3D). In addition, Δ*bphP* exhibited reduced β-1,4-endoglucanase (a type II secretion system effector) production compared with the WT and the complemented strain (Figures S3F and S3H) when grown on carboxymethyl cellulose (CMC) indicator plates (Rai et al., 2012). In a hypersensitive response (HR) assay in leaves of a non-host tomato, Δ*bphP* exhibited increased HR-like symptoms (Figure S2D). Furthermore, quantification assays indicated that Δ*bphP* exhibited elevated EPS (xanthan) production and increased attachment and biofilm formation compared with the WT or Δ*bphP*(BphP$^+$) strains (Figures 2A–2D).

Genome-wide Expression Analysis of the *Xoo*BphP Regulon in *Xoo*

To investigate the role of *Xoo*BphP in regulating global gene expression in an Indian isolate of *Xoo*, a microarray-based gene expression analysis was performed using an Agilent 8x15K array. Microarray analysis (Figure 3A) revealed that a large number of genes (534 upregulated and 512 downregulated) encoding a variety of functions (further grouped into 17 major functional categories, listed in Tables S3 and S4), had altered expression in the absence of *Xoo*BphP. In the present work, we focused further analysis on a subset of genes involved in virulence, including *egl*, *xyl* (T2SS), *hrpB4*, *hrpX*, and *hrpG* (T3SS); *sucI* and *fucP* (sugar transporters); *gumJ* (xanthan); *atsE*, *xadA*, *flg*, *mot*, and *fli* (attachment and motility); *mcp* and *che* (chemotaxis); and *htpG* and *htpX* (heat shock proteins). The finding of BphP-dependent transcription is consistent with the phenotypes described above (Figures 1A, 1B, 1F–1H, 2A–2D, 6, S1F, S1G,

(E and F) Relative quantification of expression of the xanthan biosynthesis gene *gumJ* (*Xoo3171*) and the attachment gene *XadA* (*Xoo0842*) in *Xoo* strains by real-time qRT-PCR.

(G–J). UV-vis spectra of dark-adapted (96 h) domain deletion variants of *Xoo*BphP after illumination with red, far-red, and white light.

Data in (C)–(F) are shown as the mean ± SD (n = 3); statistical significance by paired Student's t test (*$p < 0.05$, **$p < 0.01$, ***$p < 0.001$).

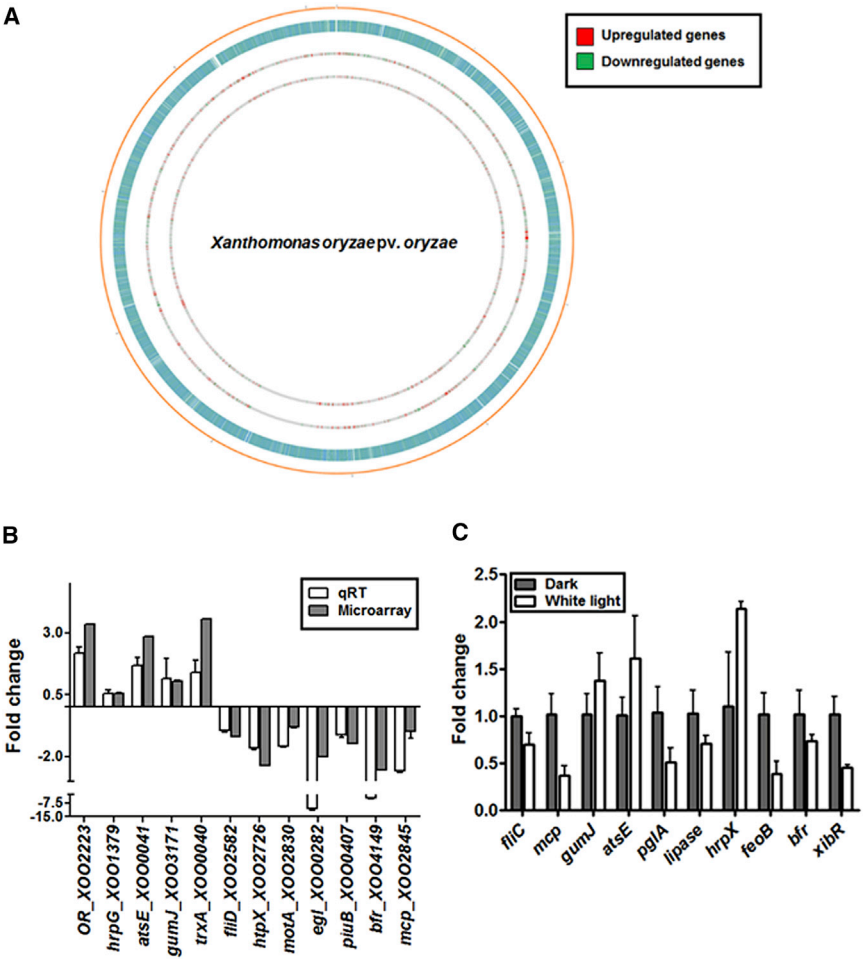

Figure 3. Genome-wide Expression Analysis of *Xoo*BphP Regulation in *Xoo*

(A) A map of differentially expressed genes in response to *XoobphP* mutation in *Xoo*, represented by a circos plot. From the outer to the inner circle, track 1 shows the circular genome of *Xoo*, track 2 shows locus presentation the of *Xoo* circular genome, and tracks 3 and 4 show differentially expressed genes in Δ*bphP* versus the *Xoo* (WT) strain and Δ*bphP* versus Δ*bphP*(BphP$^+$), grown in rich PS medium.

(B) Expression analysis by microarray and real-time qRT-PCR, indicating *Xoo*BphP regulated genes involved in flagellar biogenesis and regulation, chemotaxis, attachment, xanthan biosynthesis and biofilm, iron uptake and storage, and virulence.

(C) Relative quantification of the expression of certain *Xoo*BphP-regulated genes involved in virulence-associated functions in the WT *Xoo* strain by real-time qRT-PCR in the dark and with white light exposure.

and S3A–S3H). Genes encoding oxidoreductases, catalase, thioredoxin, and glutathione S-transferase, genes necessary for oxidative response and defense against reactive oxygen species (ROS), are produced by plants in defense of such pathogens. *Xoo*BphP-dependent genes encoding iron uptake and storage (siderophore uptake receptors; *cirA*, a TonB-dependent receptor; *bfr* [bacterioferritin]; piuB, an iron uptake factor; *fecA*, an iron-sulfur cluster; and *hemA*, *hemB*, and *hemF* [heme biosynthesis]) (An et al., 2020; Javvadi et al., 2018) suggest that *Xoo*BphP is involved in monitoring iron homeostasis in *Xoo*. *Xoo*BphP-dependent genes such as *rho*, *nusG*, and *nusA* encode general transcription machinery of the cell. This finding is consistent with the fact that Δ*bphP* differed in transcription of these genes compared with *Xoo* when assessed by qRT-PCR (Figures 2E, 2F, 3B, S2C, and S3I–S3M), further explaining the virulence deficiency of Δ*bphP*.

To validate the role of *Xoo*BphP in regulation of virulence-associated functions, we next performed expression analysis of the corresponding genes by qRT-PCR. In agreement with the phenotypic data, downregulation of genes related to flagellar motility (*flic*, *fliD*, and *motB*; Figures 3B, S3I, and S3J) and T2SS (*Xoo4035* [*cbd*], *Xoo0282* [*egl*], and *Xoo1371* [xylanase]; Figures 3B, S3K, and S3L) and upregulation of genes encoding the transcription regulator for T3SS (*hrpG* and *hrpX*; Figures 3B and S3M) and bacterial surface attachment and biofilm [*atsE*, *gumJ*, and *xadA*; Figures 3B, 2E, and 2F) were observed in the Δ*bphP* and *XoobphP*$_{C13A}$ mutants compared with the WT *Xoo* strain. Expression and phenotypic analysis of virulence-associated functions under light and dark conditions further corroborated that *Xoo*BphP is involved in light-mediated regulation of several virulence-associated functions in *Xoo* (Figure 3C; Figure S4A–S4D).

Taken together, our data further support a model where light sensing mediated by *Xoo*BphP regulates several virulence-associated functions and social behavior in *Xanthomonas*.

*Xoo*BphP Regulates Iron Uptake and Storage

In host-microbe interactions, competition for iron is critical for the outcome of infection (Cassat and Skaar, 2013; Lyles and Eichenbaum, 2018). Release of iron and BV in eukaryotic systems is driven by biliverdin reductase (Liu and Ortiz de Montellano, 2000). Recently, it has been reported that *Pseudomonas aeruginosa* BphP is involved in release of BV from the oxyferrous complex of BphO-heme during regiospecific heme cleavage (Wegele et al., 2004), suggesting that BphPs could also have a role in coordinating iron homeostasis and virulence. Interestingly, our measurements of intrinsic tryptophan fluorescence (Figure 4A) indicated that *Xoo*BphP can only bind to the ferric form of iron (K_D = 33.05 ± 1.153 μM; Figure S4E) but not the ferrous form (Figure S4F).

The Δ*bphP* mutant exhibited reduced siderophore (xanthoferrin) production when assayed on peptone sucrose agar (PSA)-chrome azurol sulfonate (CAS) siderophore indicator plates containing 75 μM of the ferrous ion chelator dipyridyl (Figure 4B) and also by quantification of siderophores, measured by

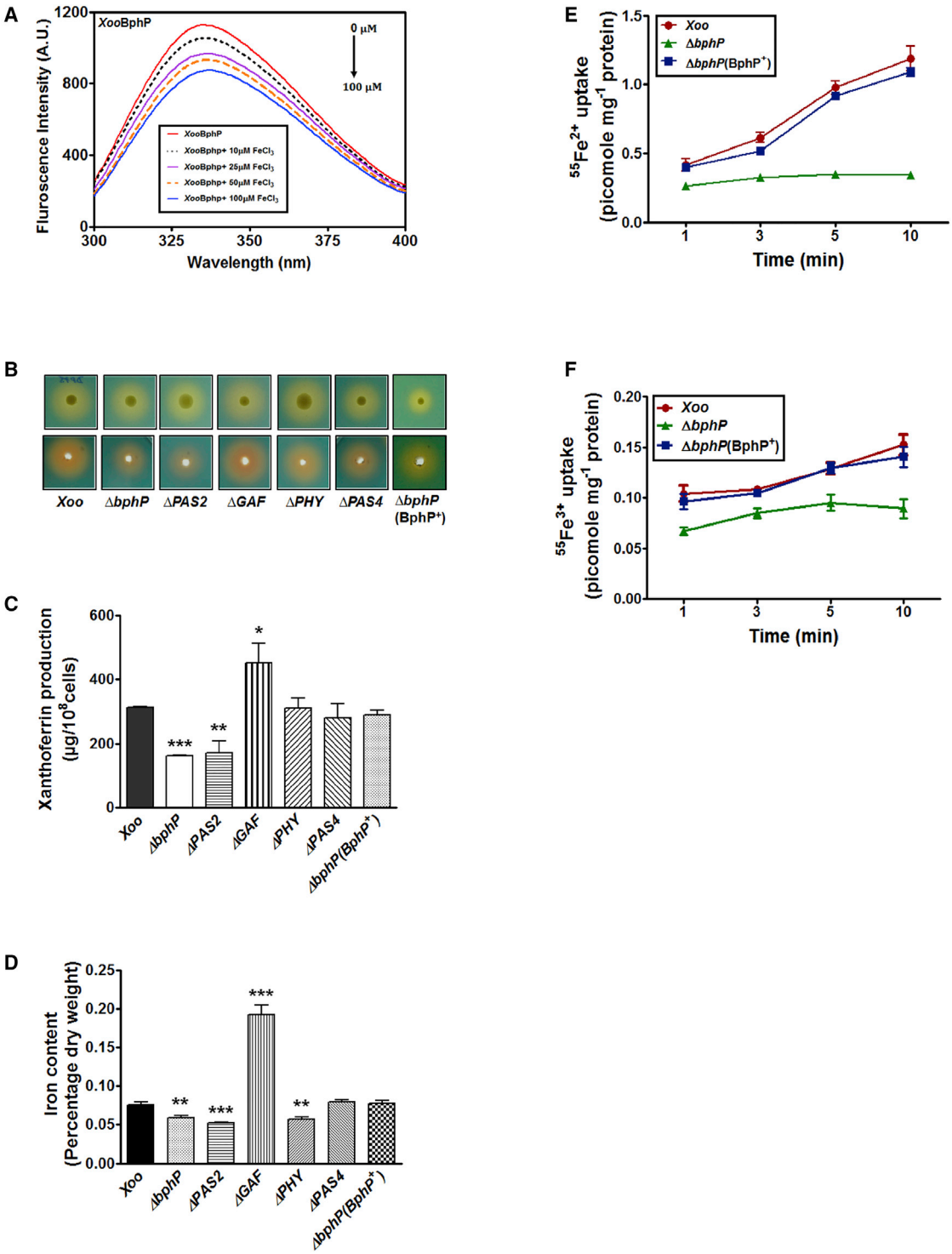

Figure 4. *Xoo*BphP Binds Specifically to the Ferric (Fe^{3+}) Form of Iron and Regulates Iron Uptake and Storage Machinery

(A) Ferric iron binding with *Xoo*BphP by intrinsic tryptophan fluorescence spectra in the presence of $FeCl_3$ (0–100 μM).

(B and C) Xanthoferrin production. Top lane: siderophore production by *Xoo* strains on PSA-CAS plates containing 75 μM ferrous iron chelator 2,2′-dipyridyl (DP). Bottom lane: siderophore isolated from cell-free culture supernatant of *Xoo* strains grown under iron-depleted condition by XAD16 affinity column chromatography.

(legend continued on next page)

reverse-phase HPLC (Figure 4C). In addition, Δ*bphP* also exhibited hyposensitivity to streptonigrin (Cohen et al., 1987; Schmitt, 1997), indicative of lower intracellular iron content (Figure S4G), which was further confirmed by measurement of the intracellular iron content by ICP-OES (inductively coupled plasma-optical emission spectrometry) (Figure 4D). Growth assays under iron-depleted conditions confirmed that the Δ*bphP* mutant exhibited reduced growth under low-iron conditions (Figure S4H). These results prompted us to investigate the role of *Xoo*BphP in iron uptake, storage, and utilization. We next performed radiolabeled iron uptake assays under iron-depleted conditions, using $^{55}Fe^{2+}$ (ferrous) and $^{55}Fe^{3+}$(ferric) forms of iron, using 10 min time course experiments (Rai et al., 2015). The Δ*bphP* mutant exhibited reduced incorporation of the ferrous and ferric forms of iron in these uptake assays (Figures 4E and 4F), indicating that *Xoo*BphP influences iron uptake and storage in *Xoo*.

To further establish a role of *Xoo*BphP in regulation of iron metabolism, we performed expression analysis of genes in these processes by qRT-PCR. Expression of genes required for iron uptake (*piuB*) and iron storage (*XOO1994* and *XOO4149* [*bfr*]) was lower in Δ*bphP* compared with the WT strain (Figure 3B).

Together, the *Xoo*BphP Domains Carry Out Photosensing and Signal Propagation

It has been proposed previously that some structural refolding along with pull/push displacement between the GAF and PHY domains in the light-inducible Pr-Pfr switch process may induce a kink and rotation of the output module positions, leading to signal propagation from the photosensory triad to the output module (Burgie et al., 2014; Takala et al., 2015; Otero et al., 2016).

To understand whether the virulence deficiency exhibited by each individual domain deletion mutant is due to altered light signal propagation, we overexpressed and purified individual domain deletion proteins (*Xoo*BphPΔPAS2, *Xoo*BphPΔGAF, *Xoo*BphPΔPHY, and *Xoo*BphPΔPAS4; Figure S1D) as N-terminal His-tagged variants (Figure S1E). UV-vis absorption experiments revealed that *Xoo*BphPΔPAS2 and *Xoo*BphPΔGAF did not exhibit any photo-inducible Pr-Pfr changes because of the absence of Cys^{13} and lyase activity, respectively (Figures 2G and 2H). Interestingly, *Xoo*BphPΔPHY was found only in the Pr state, and no red and/or darkness conversion to the Pfr state was observed (Figure 2I). However, *Xoo*BphPΔPAS4 exhibited photoconversion somewhat similar to the native *Xoo*BphP (Figure 2J). The PAS2-GAF-PHY domain triad thus appears to contribute to the light signal perception of *Xoo*BphP, and PAS4 might be responsible for structural stability of the native protein (Otero et al., 2016).

*Xoo*BphP Modulates Intracellular c-di-GMP Levels in a Light-Dependent Fashion via an EAL Motif that Is Conserved in *Xanthomonads*

In general, most biological photoreceptors, including phytochromes, exhibit kinase or phosphatase activity as effector functions. However, sequence analysis of *Xoo*BphP and bacteriophytochromes from several bacteria indicated that, similar to *Xanthomonas*, BphPs from several other bacteria, such as *Bradyrhizobium* and *Rhodopseudomonas*, do not have similarity to any known or predictable output or effector domains (Figure S2A; Bonomi et al., 2016; Auldridge and Forest, 2011).

The GAF domains from the sensory module of other BphPs have been reported to be involved in modulating the cellular levels of c-NMP and consequently bind to a wide range of effector modules and thereby control diverse cellular functions (Heikaus et al., 2009; Hengge, 2009). In order to investigate the *Xoo*BphP signal transduction mechanism, His-tagged *Xoo*BphP was probed for enzymatic activity toward several known substrates that are generally utilized by the output or effector domains of bacterial photoreceptors. Interestingly, the *Xoo*BphP did not exhibit any detectable activity toward indicator substrates such as ATP. However, *Xoo*BphP exhibited phosphodiesterase (PDE) activity with the substrate bis-*p*-nitrophenyl phosphate (bis-*p*NPP) in the presence of Mn^{2+} (Chen et al., 2004; Nagata et al., 2008). In addition, the *Xoo*BphPΔPAS2, *Xoo*BphPΔPHY, and *Xoo*BphPΔPAS4 domain deletion proteins also exhibited similar PDE activity against bis-*p*NPP as a substrate as the native *Xoo*BphP (Figures 5A and S5A). The *Xoo*BphPΔGAF and *Xoo*BphPC13A mutants exhibited higher PDE activity compared with the WT protein under these assay conditions (Figures 5A and S5A). *Xoo*BphP was then assayed for PDE activity using potential cellular substrates such as cGMP and c-di-GMP by detecting degradation products by reverse-phase HPLC. Interestingly, *Xoo*BphP exhibited activity specifically toward c-di-GMP, generating a compound with similar retention time as GMP (Figure 5B), which was analyzed by comparing the HPLC chromatogram with standards (Figure S5B). PDE activity was further confirmed by mass spectrometry of this product, which exhibited a mass identical to the GMP standard. No detectable PDE activity was observed with cGMP as substrate (Figure S5C).

c-di-GMP-specific PDE activity is exhibited by proteins containing an EAL or HD-GYP domain, modulating the cytosolic c-di-GMP level by generating linear dinucleotide pGpG or GMP (Jenal and Malone 2006; Sondermann et al., 2012; Römling et al., 2013). Sequence analysis of *Xoo*BphP did not reveal a HD-GYP motif (Figure S2B). However, an EAL motif was present on an α helix stretch located between the PAS2 and GAF domains at the N terminus (Figure S2B).

Furthermore, the glutamic acid residue (Glu^{131}) of the putative EAL motif is well conserved among different *Xanthomonas* species (Figure S2A). To determine whether the conserved glutamic acid (E131) is responsible for the PDE activity, a *Xoo*BphPE131A variant (Glu^{131} replaced with Ala; Figure S1D) was constructed and purified (Figure S1E). *Xoo*BphPE131A did not exhibit any PDE activity against bis-*p*NPP (Figure 5A) and was also unable

(C) Xanthoferrin quantification by reverse-phase HPLC using a standard curve generated from known concentrations of pure vibrioferrin.
(D) Intracellular iron content of *Xoo* strains, measured by ICP-OES.
(E and F). *In-vitro*-radiolabeled $^{55}Fe^{2+}$ and $^{55}Fe^{3+}$ uptake under iron-depleted condition during a 10-min time course.
Data in (C) and (D) are shown as the mean ± SD (n = 3); statistical significance by paired Student's t test (*p < 0.05, **p < 0.01, ***p < 0.001).

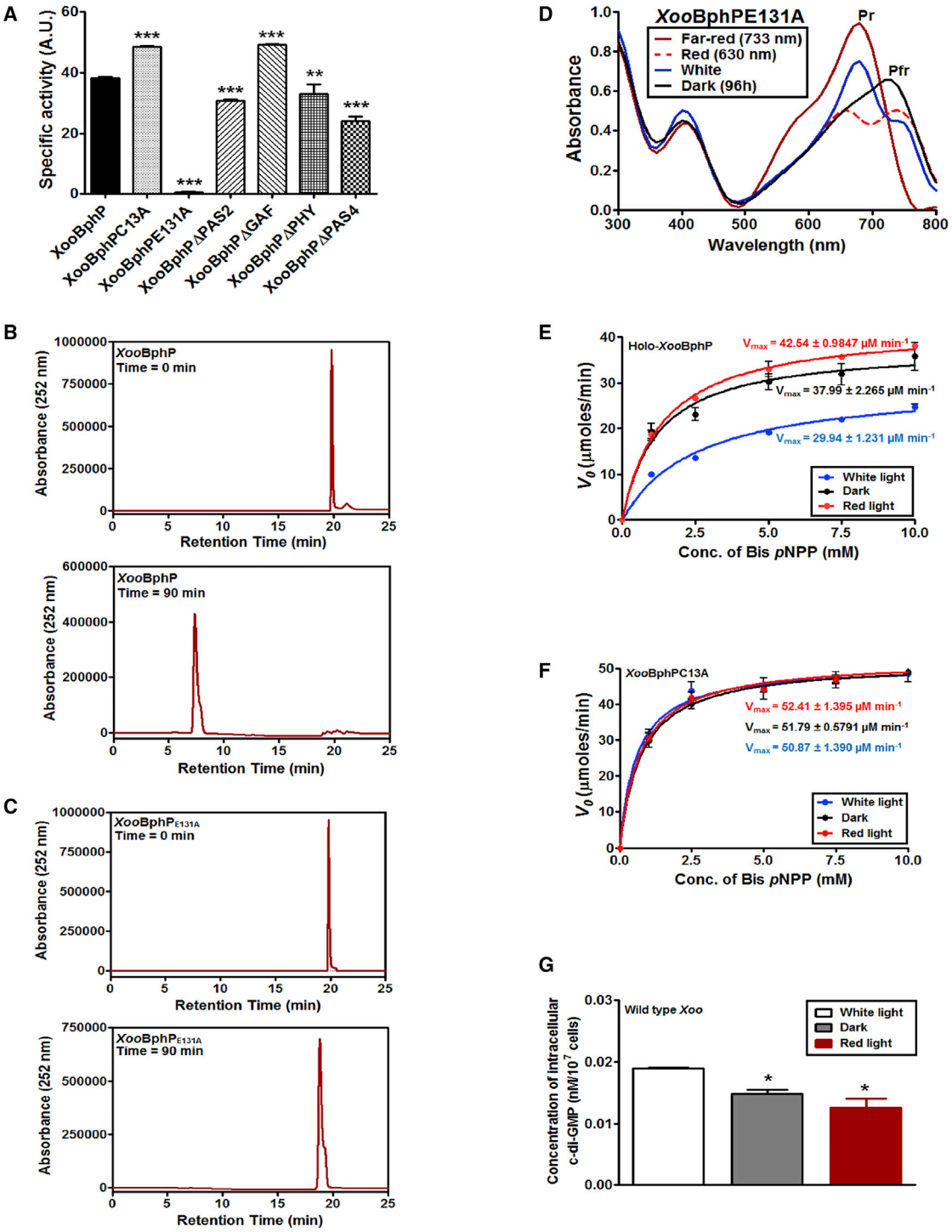

Figure 5. *Xoo*BphP Modulates Cytosolic c-di-GMP Concentration by Intrinsic PDE Activity Executed by Its EAL Motif in a Light-Dependent Manner

(A) PDE-specific activity of *Xoo*BphP and variants by intrinsic Trp fluorescence spectroscopy.

(B and C) HPLC chromatograms of aliquots of reaction mixtures containing 10 μM of c-di-GMP followed by immediate boiling after addition of *Xoo*BphP and *Xoo*BphPE131A at 0 min and after 90 min.

(legend continued on next page)

to degrade c-di-GMP to GMP; we could not detect any degradation product including a GMP-specific peak in reverse-phase HPLC analysis of the reaction product (Figure 5C). However, *Xoo*BphPE131A exhibited photoconversion similar to native *Xoo*BphP (Figure 5D).

We then sought to examine whether the c-di-GMP-specific PDE activity of *Xoo*BphP is light dependent. To test this *in vitro*, the PDE activity for native *Xoo*BphP and the light-insensitive variant (*Xoo*BphPC13A) was measured under dark and light conditions. Interestingly, *Xoo*BphP exhibited significantly higher PDE activity (V_{max} = 42.54 ± 0.98 μM min^{-1}) when exposed to red light or darkness compared with white light (V_{max} = 29.9 ± 1.23 μM min^{-1}) (Figure 5E). Importantly, *Xoo*BphPC13A did not exhibit significant differences in PDE activity under the different light conditions (Figure 5F).

Furthermore, measurement of the intracellular concentration of c-di-GMP in the WT *Xoo* strain exposed to different light conditions revealed that *Xoo* exhibited lower intracellular c-di-GMP levels under dark conditions and after red light exposure compared with exposure to white light (Figure 5G).

Collectively, these results strongly indicate that *Xoo*BphP modulates the intracellular c-di-GMP concentration in a light-dependent fashion via the EAL motif, which is conserved among *Xanthomonas* species.

*Xoo*BphP Integrates Photo-sensing and Intracellular c-di-GMP Levels to Coordinate Social Behavior to Promote Entry, Colonization, and Virulence

To further establish a role of *Xoo*BphP in light sensing as well as modulation of intracellular c-di-GMP signaling to control social behavior in *Xoo*, we generated a mutant strain of *Xoo* harboring the *XoobphP*$_{E131A}$ (Ala substituting Glu^{131}) mutant allele incorporated into the *XoobphP* genomic locus. We also ectopically expressed a His-tagged EAL-PDE-encoding gene, *PA3947*, from *Pseudomonas aeruginosa* PA01(Deng et al., 2012) in the Δ*bphP* background (Δ*bphP*:: PA3947). Immunoblot analysis with an anti-His antibody confirmed the size and expression of PA3947 (Figure S5D). We then assessed the infectivity of these strains as well as expression of virulence-associated functions.

XoobphP$_{E131A}$ exhibited reduced infectivity of rice in wound inoculation and topical inoculation, similar to that of Δ*bphP* (Figures 6A and S5E). Interestingly, ectopic expression of PA3947 rescued the virulence deficiency exhibited by Δ*bphP* in wound infection (Figures 6A and 6B) but was unable to rescue virulence, as assessed by topical inoculation of leaves (Figures S5E and S5F).

Furthermore, *XoobphP*$_{E131A}$ exhibited reduced motility and chemotaxis responses (Figures 6D, 6E, and S5G) and reduced xanthoferrin production and iron uptake (Figures 6D, 6H, and S5H) but enhanced xanthan production (Figures 6D and 6F) and biofilm formation (Figures 6D and 6G), similar to that of Δ*bphP*. Ectopic expression of PA3947 in Δ*bphP* could rescue siderophore production, iron uptake, and xanthan and biofilm formation but was unable to rescue motility and chemotaxis of Δ*bphP* and *XoobphP*$_{E131A}$ (Figures 6D–6H and S5E–S5H). In addition, measurement of the intracellular c-di-GMP levels indicated that Δ*bphP* and *XoobphP*$_{E131A}$ exhibited significantly higher levels of cellular c-di-GMP compared with the WT *Xoo* strain (Figure 6C). However, ectopic expression of PA3947 reduced the levels of c-di-GMP to similar levels as in the WT *Xoo* strain (Figure 6C).

We thus conclude that *Xoo*BphP has an important role in pathogenic lifestyle transition involving entry, colonization, and virulence by integrating environmental light-sensing and intracellular c-di-GMP signaling to fine-tune many social behaviors and vital functions (Figure 7).

DISCUSSION

Bacteria coordinate several traits in response to different environmental signals that fine-tune cellular processes to facilitate transition from a planktonic motile to a sessile lifestyle. In this study, we demonstrate that the non-photosynthetic phytopathogen *Xoo* coordinates several social behaviors by sensing distinct light signals through a photo-sensing, bathy-type bacteriophytochrome, *Xoo*BphP. Our results demonstrate that *Xoo*BphP-mediated light perception promotes virulence, motility, and chemotaxis-mediated entry and colonization of plants in response to red light and dark conditions. Our results suggest that specific wavelengths of light act as distinctive environmental stimuli that induce conformational changes in bacteriophytochromes, which leads to altered signal transduction/propagation, changing the expression of several cellular processes.

Bacteriophytochromes in many non-photosynthetic and plant-associated bacteria, such as *Xanthomonas*, *Bradyrhizobium*, *Rhodopseudomonas*, and *Pseudomonas*, lack effector/output domains or harbor a histidine kinase-like domain lacking a receiver (Rec) module that is required for interaction with the cognate response regulator (van der Horst et al., 2007; Kiang et al., 2007; Idnurm and Crosson, 2009; Beattie et al., 2018).

Our work reveals that *Xoo*BphP perceives light through N-terminal photo-sensory domains and integrates the light signal to modulate c-di-GMP-specific PDE activity. We provide evidence that various light conditions differentially alter the PDE activity of the native *Xoo*BphP, whereas the light-insensitive *Xoo*BphP$_{C13A}$ mutant does not exhibit any significant change in PDE activity when exposed to different types of light (Figures 5E and 5F). Previous structural studies have proposed that bacteriophytochromes can undergo conformational changes during photoconversion, which may result in a distinct three-dimensional position of the domains (Otero et al., 2016). It seems likely that such photoconversion, resulting in formation of a Pfr state under dark conditions and under

(D) UV-vis spectra of dark-adapted and illuminated *Xoo*BphPE131A.
(E and F) Catalytic activity of *Xoo*BphP and *Xoo*BphPC13A as a function of bis-*p*NPP concentrations (Michaelis-Menten plot).
(G) *In vivo* cytosolic concentration of c-di-GMP by HPLC under different light conditions.
Data in (A) and (G) are shown as the mean ± SD (n = 3); statistical significance by paired Student's t test (*p < 0.05, **p < 0.01, ***p < 0.001).

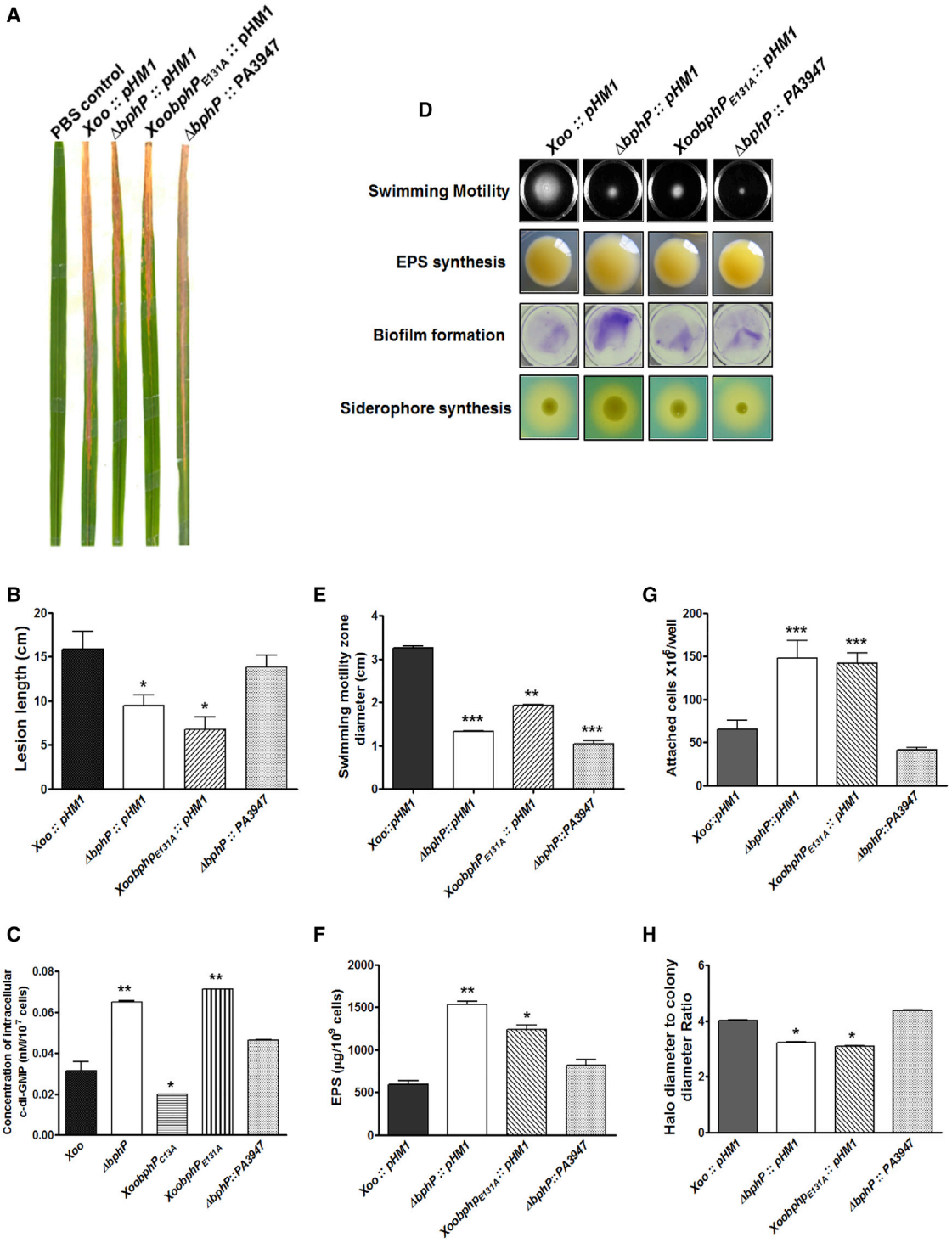

Figure 6. *Xoo*BphP Regulates the Downstream Light-Signaling Cascade through Light-Dependent Cytosolic c-di-GMP Concentration Modulation

(A and B) 14 dpi BLB lesion symptoms of rice leaves of wound inoculation by the leaf clipping method. Δ*bphP*::PA3947 represents the *XoobphP* null mutant ectopically expressing PA3947 (EAL-containing protein) in pHM1 from *Pseudomonas aeruginosa* PA01 and 14 dpi mean lesion lengths. Data are shown as mean ± SD (n = 25).

(C) *In vivo* level of c-di-GMP determined by HPLC. Data are shown as the mean ± SD (n = 3).

(D) Determination of virulence-associated traits, swimming motility, and EPS and biofilm production.

(legend continued on next page)

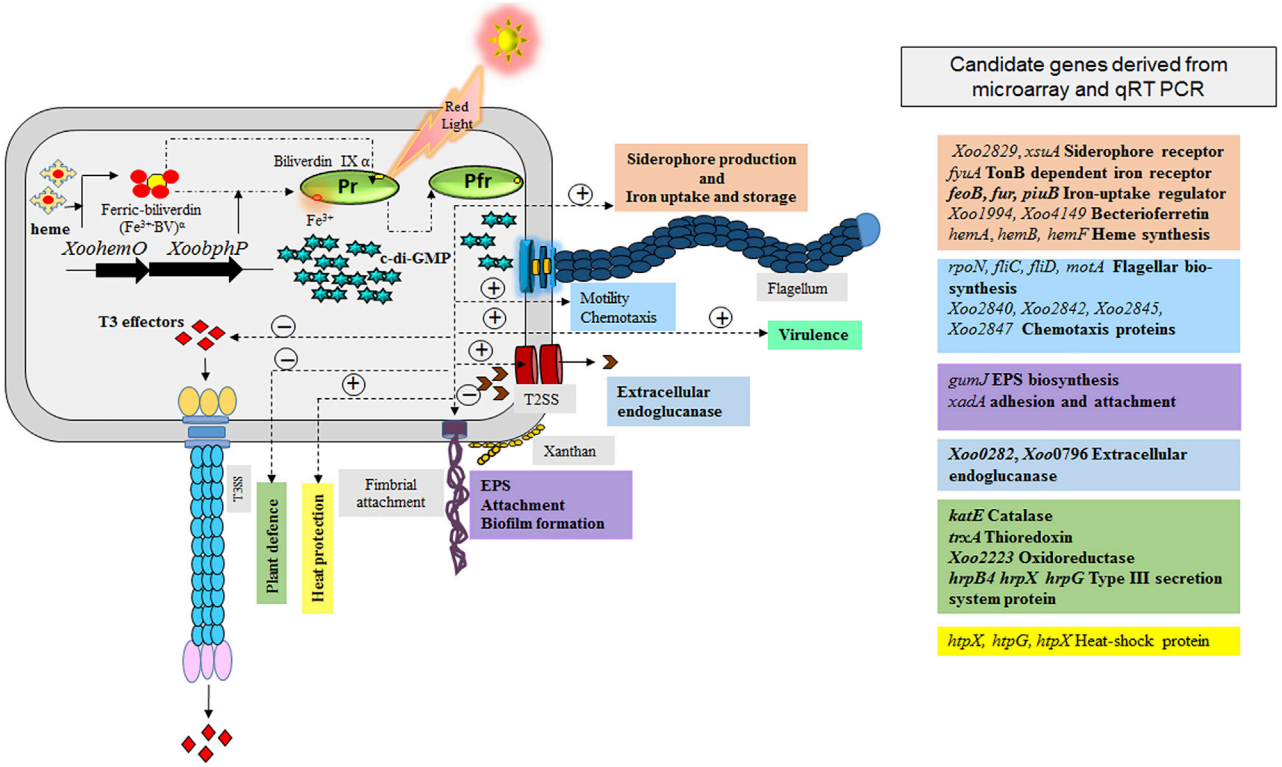

Figure 7. A Proposed Model Showing Mechanistic Insights into *Xoo*BphP-Mediated Light Signaling

During daytime (white light), *Xoo*BphP exists in the Pr state, and *Xanthomonas* forms a biofilm-like structure for protection from the hostile phyllosphere environment. At dusk, *Xoo*BphP senses red light and photoconverts to the Pfr state, which is maintained throughout the night (dark). *Xoo*BphP-Pfr, because of its elevated c-di-GMP-specific PDE activity, has a lower cytosolic c-di-GMP level, which in turn, increases sessile-to-motile transition. + and − indicate positive regulation and negative regulation, respectively.

red light irradiation, leads to more solution exposure of the EAL, resulting in elevated PDE activity of the protein, which, in turn, results in a drop in intracellular c-di GMP concentration. Similarly, white light and far-red exposure can convert Pfr back to the Pr state, leading to a less solution-exposed conformation of EAL, in turn leading to less PDE activity and, hence, higher intracellular c-di-GMP levels. Similar light-regulated PDE activity of the bacteriophytochrome BlrP1 in *Klebsiella pneumonia* has been reported previously (Barends et al., 2009).

Our results of ectopic expression of a *Pseudomonas aeruginosa* EAL-containing PDE protein in the *XoobphP* deletion mutant suggest that photo-sensing-mediated modulation of PDE activity is employed by *Xoo*BphP through its photosensor-linked EAL motif but not by other light-independent PDEs. In agreement with this model, it has been shown previously that binding of oxygen to the sensor domain (which is associated with the EAL domain containing c-di-GMP PDE) regulates its PDE activity in *Gluconacetobacter xylinus* (Chang et al., 2001). It is pertinent that, in several bacteria, sensing of diverse signals, such as O_2, NO, CO, and the redox state, by sensory domains associated with c-di-GMP-metabolizing enzymes modulates their enzymatic activity (Schirmer and Jenal, 2009, Jenal and Malone, 2006; Sondermann et al., 2012; Römling et al., 2013).

During dusk, long-wavelength red light reaches the surface of the earth in a higher proportion than shorter-wavelength blue light, which is subject to higher scattering (Beattie et al., 2018; Santamaría-Hernando et al., 2018). Circadian clocks modulate various physiological processes, including defense responses in plants and animals (Scheiermann et al., 2013; Cheng et al., 2019). The host plant temporally coordinates expression of defense-related genes via circadian clock, maximizing expression of such genes at the most likely time of pathogen attack (Bhardwaj et al., 2011; Wang et al., 2011; Zhang et al., 2013). The intensity of host defense is typically lower at dusk and at night compared with daytime (Sharma and Bhatt, 2015; Cheng et al.,

(E) Quantification of motility zone diameter.
(F) Quantitative measurement of EPS production using the phenol-sulfuric acid colorimetric method.
(G) Quantification of attached cells in the static biofilm after 48 h of growth.
(H) Quantification of siderophore production by calculating the average ratio of siderophore halo to colony diameter on PSA-CAS plates containing 75 μM DP. Error bars represent SD of the mean (n = 3); statistical significance by paired Student's t test (*p < 0.05, **p < 0.01, ***p < 0.001).

2019). Pathogens such as *Xoo* reside on the hostile surface of rice leaves and obviously encounter this diurnal cycle of light quantity and quality. The humid and cooler conditions predominating at night promote accumulation of hydathodal fluid, which facilitates invasion of vascular tissue through hydathodes by pathogens such as *Xoo* (An et al., 2020; Noda and Kaku, 1999). We propose that, under conditions of red light predominating at dusk, *Xoo*BphP-Pfr is formed and is maintained throughout the night (dark conditions). *Xoo*BphP-Pfr causes the pathogen to increase expression of virulence-associated functions, resulting in successful active invasion into the host vasculature, a process that also coincides with a lessened host response to the pathogen, further increasing the likelihood of successful infection. We further speculate that, during the day, white light induces photoconversion of Pfr to the Pr form of *Xoo*BphP, enabling the pathogen to attenuate virulence gene expression when the host defenses are maximally active (Sharma and Bhatt, 2015; Cheng et al., 2019).

Xanthomonas leads a hemibiotrophic lifestyle; it forms biofilm-like structures on plant surfaces that have been proposed to protect the cells in the inhospitable phyllosphere environment (Zarei et al., 2018; An et al., 2020; Kumar Verma et al., 2018; Niño-Liu et al., 2006). In this study, we demonstrate that *Xoo*BphP promotes light-dependent motility and chemotaxis under red light as well as in the dark while suppressing EPS and biofilm formation under these conditions. Cellular c-di-GMP levels, in turn, have a key role in regulating motility, EPS production, and biofilm formation in this light-dependent lifestyle transition (Bernier et al., 2011; Jenal and Malone, 2006; Valentini and Filloux, 2016). This study suggests that, during daytime, white light facilitates accumulation of higher levels of cellular c-di-GMP (because of lower PDE activity of *Xoo*BphP), promoting biofilm formation and a sessile, stress-tolerant lifestyle on plant surfaces. However, at dusk and at night, the higher PDE activity of XooBphP leads to lower intracellular levels of c-di-GMP, promoting chemotaxis-driven motility and expression of virulence-associated functions.

In many pathogenic bacteria, including *Xanthomonas*, iron homeostasis has an important role in coordinating virulence (Andrews et al., 2003; Braun and Killmann, 1999; Pandey et al., 2016). Our work reveals that *Xoo*BphP regulates expression of iron uptake and storage in *Xoo* (Figure 3B; Table S3) because the Δ*bphP* and *XoobphP*$_{E131A}$ mutants were deficient in siderophore production and iron uptake and, therefore, had low internal iron levels.

Moreover, *Xoo*BphP can specifically bind ferric iron. *Xoo*BphP is unlikely to function as an iron reservoir as bacterioferritins do because it does not bear any homology to such iron storage proteins. It is, however, possible that *Xoo*BphP acts as a ferric ion, sequestering molecule needed during breakdown of ferric BV complexes by *Xoo*BphO (Wegele et al., 2004) and synthesis of BV, the chromophore utilized by *Xoo*BphP.

This study reveals that light can act as a key signal for lifestyle transition in a nonphotosynthetic bacterial pathogen and that bacteriophytochromes can mediate light sensing and modulation of a widely conserved second messenger to regulate diverse behaviors and coordination of virulence functions to enable successful colonization of a host.

STAR★METHODS

Detailed methods are provided in the online version of this paper and include the following:

- KEY RESOURCES TABLE
- RESOURCE AVAILABLITY
  - Lead Contact
  - Materials Availability
  - Data and Code Availability
- EXPERIMENTAL MODEL AND SUBJECT DETAILS
  - Bacterial strains
  - Bacterial mutant and complemented strain generation
- METHOD DETAILS
  - Molecular biology techniques
  - Site directed mutagenesis
  - Cloning, overexpression and purification of His-tagged XooBphP and its variants
  - UV–vis spectroscopy
  - Swimming motility assay
  - Quantitative chemotaxis assay by syringe capillary method
  - *In planta* Virulence assays on rice leaves
  - Migration of X. oryzae pv. oryzae inside the leaves
  - Extracellular Enzyme assay
  - Separation and quantification of EPS
  - Static biofilm and attachment assay
  - Growth assay
  - CAS plate assays for siderophore production
  - Siderophore estimation by HPLC
  - SNG sensitivity assay
  - Determination of intracellular iron concentration by ICP-OES
  - Iron uptake assay
  - Intrinsic tryptophan fluorescence
  - PDE activity assay
  - Cyclic nucleotide phosphodiesterase activity by HPLC
  - Extraction and quantification of intracellular c-di-GMP
  - Hypersensitive response assay
  - Cell fractionation
  - Expression analysis by qRT PCR
  - Gene expression profiling using Agilent microarray platform
- QUANTIFICATION AND STATISTICAL ANALYSIS

SUPPLEMENTAL INFORMATION

Supplemental Information can be found online at https://doi.org/10.1016/j.celrep.2020.108202.

ACKNOWLEDGMENTS

We thank S.S. Pandey for help with microarray data analysis and R.N. Mishra, CDFD, for preparing the customized lightbox. R.K.V. is a recipient of senior research fellowships from the Department of Biotechnology, India. The DBT-RA Program in Biotechnology and Life Sciences is gratefully acknowledged for financial support (to A.B.). This study was supported by grants from DBT Plant Sciences, the Government of India, DST-SERB, a National Bioscience Award for Carrier Development, and DBT and CDFD core funds (to S.C.).

AUTHOR CONTRIBUTIONS

R.K.V. and A.B. performed all experiments, analyzed data, and contributed to figure preparation and writing and editing of the draft manuscript. B.B.P. performed the motility assay. S.K.L. contributed to localization and western blotting. A.K. constructed ectopic c-di-GMP constructs. R.K.V. and A.B. contributed to experimental design. S.C. conceptualized and designed experiments and edited and contributed to writing the manuscript.

DECLARATION OF INTERESTS

The authors declare no competing interests.

Received: March 2, 2020
Revised: June 13, 2020
Accepted: September 4, 2020
Published: September 29, 2020

REFERENCES

An, S.Q., Potnis, N., Dow, M., Vorhölter, F.J., He, Y.Q., Becker, A., Teper, D., Li, Y., Wang, N., Bleris, L., and Tang, J.L. (2020). Mechanistic insights into host adaptation, virulence and epidemiology of the phytopathogen Xanthomonas. FEMS Microbiol. Rev. *44*, 1–32.

Andrews, S.C., Robinson, A.K., and Rodríguez-Quiñones, F. (2003). Bacterial iron homeostasis. FEMS Microbiol. Rev. *27*, 215–237.

Auldridge, M.E., and Forest, K.T. (2011). Bacterial phytochromes: more than meets the light. Crit. Rev. Biochem. Mol. Biol. *46*, 67–88.

Barends, T.R., Hartmann, E., Griese, J.J., Beitlich, T., Kirienko, N.V., Ryjenkov, D.A., Reinstein, J., Shoeman, R.L., Gomelsky, M., and Schlichting, I. (2009). Structure and mechanism of a bacterial light-regulated cyclic nucleotide phosphodiesterase. Nature *459*, 1015–1018.

Barkovits, K., Harms, A., Benkartek, C., Smart, J.L., and Frankenberg-Dinkel, N. (2008). Expression of the phytochrome operon in Pseudomonas aeruginosa is dependent on the alternative sigma factor RpoS. FEMS Microbiol. Lett. *280*, 160–168.

Beattie, G.A., Hatfield, B.M., Dong, H., and McGrane, R.S. (2018). Seeing the light: the roles of red- and blue-light sensing in plant microbes. Annu. Rev. Phytopathol. *56*, 41–66.

Bernier, S.P., Ha, D.G., Khan, W., Merritt, J.H., and O'Toole, G.A. (2011). Modulation of Pseudomonas aeruginosa surface-associated group behaviors by individual amino acids through c-di-GMP signaling. Res. Microbiol. *162*, 680–688.

Bhardwaj, V., Meier, S., Petersen, L.N., Ingle, R.A., and Roden, L.C. (2011). Defence responses of Arabidopsis thaliana to infection by Pseudomonas syringae are regulated by the circadian clock. PLoS ONE *6*, e26968.

Biswas, A., Mandal, S., and Sau, S. (2014). The N-terminal domain of the repressor of Staphylococcus aureus phage Φ11 possesses an unusual dimerization ability and DNA binding affinity. PLoS ONE *9*, e95012.

Biswas, A., Mandal, S., and Sau, S. (2017). Identification and characterization of a CI binding operator at a distant location in the temperate staphylococcal phage ϕ11. FEMS Microbiol. Lett. *364*, fnx201.

Biswas, A., Ghosh, S., Sinha, D., Dutta, A., Seal, S., Bagchi, A., and Sau, S. (2019). Dimerization ability, denaturation mechanism, and the stability of a staphylococcal phage repressor and its two domains. Int. J. Biol. Macromol. *124*, 903–914.

Bogdanove, A.J., Koebnik, R., Lu, H., Furutani, A., Angiuoli, S.V., Patil, P.B., Van Sluys, M.A., Ryan, R.P., Meyer, D.F., Han, S.W., et al. (2011). Two new complete genome sequences offer insight into host and tissue specificity of plant pathogenic Xanthomonas spp. J. Bacteriol. *193*, 5450–5464.

Bonomi, H.R., Toum, L., Sycz, G., Sieira, R., Toscani, A.M., Gudesblat, G.E., Leskow, F.C., Goldbaum, F.A., Vojnov, A.A., and Malamud, F. (2016). Xanthomonas campestris attenuates virulence by sensing light through a bacteriophytochrome photoreceptor. EMBO Rep. *17*, 1565–1577.

Bradford, M.M. (1976). A rapid and sensitive method for the quantitation of microgram quantities of protein utilizing the principle of protein-dye binding. Anal. Biochem. *72*, 248–254.

Braun, V., and Killmann, H. (1999). Bacterial solutions to the iron-supply problem. Trends Biochem. Sci. *24*, 104–109.

Burgie, E.S., Wang, T., Bussell, A.N., Walker, J.M., Li, H., and Vierstra, R.D. (2014). Crystallographic and electron microscopic analyses of a bacterial phytochrome reveal local and global rearrangements during photoconversion. J. Biol. Chem. *289*, 24573–24587.

Büttner, D., and Bonas, U. (2010). Regulation and secretion of Xanthomonas virulence factors. FEMS Microbiol. Rev. *34*, 107–133.

Cassat, J.E., and Skaar, E.P. (2013). Iron in infection and immunity. Cell Host Microbe *13*, 509–519.

Chang, A.L., Tuckerman, J.R., Gonzalez, G., Mayer, R., Weinhouse, H., Volman, G., Amikam, D., Benziman, M., and Gilles-Gonzalez, M.A. (2001). Phosphodiesterase A1, a regulator of cellulose synthesis in Acetobacter xylinum, is a heme-based sensor. Biochemistry *40*, 3420–3426.

Chatterjee, S., and Sonti, R.V. (2002). rpfF mutants of Xanthomonas oryzae pv. oryzae are deficient for virulence and growth under low iron conditions. Mol. Plant Microbe Interact. *15*, 463–471.

Chen, L., Wu, W., Dentchev, T., Zeng, Y., Wang, J., Tsui, I., Tobias, J.W., Bennett, J., Baldwin, D., and Dunaief, J.L. (2004). Light damage induced changes in mouse retinal gene expression. Exp. Eye Res. *79*, 239–247.

Cheng, Y.T., Zhang, L., and He, S.Y. (2019). Plant-Microbe Interactions Facing Environmental Challenge. Cell Host Microbe *26*, 183–192.

Cohen, M.S., Chai, Y., Britigan, B.E., McKenna, W., Adams, J., Svendsen, T., Bean, K., Hassett, D.J., and Sparling, P.F. (1987). Role of extracellular iron in the action of the quinone antibiotic streptonigrin: mechanisms of killing and resistance of Neisseria gonorrhoeae. Antimicrob. Agents Chemother. *31*, 1507–1513.

Davis, S.J., Vener, A.V., and Vierstra, R.D. (1999). Bacteriophytochromes: phytochrome-like photoreceptors from nonphotosynthetic eubacteria. Science *286*, 2517–2520.

Davis, S.J., Bhoo, S.H., Durski, A.M., Walker, J.M., and Vierstra, R.D. (2001). The heme-oxygenase family required for phytochrome chromophore biosynthesis is necessary for proper photomorphogenesis in higher plants. Plant Physiol. *126*, 656–669.

Deng, Y., Schmid, N., Wang, C., Wang, J., Pessi, G., Wu, D., Lee, J., Aguilar, C., Ahrens, C.H., Chang, C., et al. (2012). Cis-2-dodecenoic acid receptor RpfR links quorum-sensing signal perception with regulation of virulence through cyclic dimeric guanosine monophosphate turnover. Proc. Natl. Acad. Sci. USA *109*, 15479–15484.

Dow, M. (2008). Diversification of the function of cell-to-cell signaling in regulation of virulence within plant pathogenic xanthomonads. Sci. Signal. *1*, pe23.

Finn, R.D., Bateman, A., Clements, J., Coggill, P., Eberhardt, R.Y., Eddy, S.R., Heger, A., Hetherington, K., Holm, L., Mistry, J., et al. (2014). Pfam: the protein families database. Nucleic Acids Res. *42*, D222–D230.

Giraud, E., Fardoux, J., Fourrier, N., Hannibal, L., Genty, B., Bouyer, P., Dreyfus, B., and Verméglio, A. (2002). Bacteriophytochrome controls photosystem synthesis in anoxygenic bacteria. Nature *417*, 202–205.

Giraud, E., Zappa, S., Vuillet, L., Adriano, J.M., Hannibal, L., Fardoux, J., Berthomieu, C., Bouyer, P., Pignol, D., and Verméglio, A. (2005). A new type of bacteriophytochrome acts in tandem with a classical bacteriophytochrome to control the antennae synthesis in Rhodopseudomonas palustris. J. Biol. Chem. *280*, 32389–32397.

Hauck, P., Thilmony, R., and He, S.Y. (2003). A Pseudomonas syringae type III effector suppresses cell wall-based extracellular defense in susceptible Arabidopsis plants. Proc. Natl. Acad. Sci. U.S.A. *100*, 8577–8582.

Heikaus, C.C., Pandit, J., and Klevit, R.E. (2009). Cyclic nucleotide binding GAF domains from phosphodiesterases: structural and mechanistic insights. Structure *17*, 1551–1557.

Hengge, R. (2009). Principles of c-di-GMP signalling in bacteria. Nat. Rev. Microbiol. *7*, 263–273.

Idnurm, A., and Crosson, S. (2009). The photobiology of microbial pathogenesis. PLoS Pathog. *5*, e1000470.

Jana, B., Bandhu, A., Mondal, R., Biswas, A., Sau, K., and Sau, S. (2012). Domain structure and denaturation of a dimeric Mip-like peptidyl-prolyl cis-trans isomerase from Escherichia coli. Biochemistry *51*, 1223–1237.

Jaubert, M., Vuillet, L., Hannibal, L., Adriano, J.M., Fardoux, J., Bouyer, P., Bonaldi, K., Fleischman, D., Giraud, E., and Verméglio, A. (2008). Control of peripheral light-harvesting complex synthesis by a bacteriophytochrome in the aerobic photosynthetic bacterium Bradyrhizobium strain BTAi1. J. Bacteriol. *190*, 5824–5831.

Javvadi, S., Pandey, S.S., Mishra, A., Pradhan, B.B., and Chatterjee, S. (2018). Bacterial cyclic β-(1,2)-glucans sequester iron to protect against iron-induced toxicity. EMBO Rep. *19*, 172–186.

Jenal, U., and Malone, J. (2006). Mechanisms of cyclic-di-GMP signaling in bacteria. Annu. Rev. Genet. *40*, 385–407.

Kauffman, H.E. (1973). An improved technique for evaluat-ing resistance of rice varieties to Xanthomonas oryzae. Plant Dis. Rep. *57*, 537–541.

Kiang, N.Y., Siefert, J., Govindjee, and Blankenship, R.E. (2007). Spectral signatures of photosynthesis. I. Review of Earth organisms. Astrobiology *7*, 222–251.

Kumar Verma, R., Samal, B., and Chatterjee, S. (2018). Xanthomonas oryzae pv. oryzae chemotaxis components and chemoreceptor Mcp2 are involved in the sensing of constituents of xylem sap and contribute to the regulation of virulence-associated functions and entry into rice. Mol. Plant Pathol. *19*, 2397–2415.

Liu, Y., and Ortiz de Montellano, P.R. (2000). Reaction intermediates and single turnover rate constants for the oxidation of heme by human heme oxygenase-1. J. Biol. Chem. *275*, 5297–5307.

Lyles, K.V., and Eichenbaum, Z. (2018). From host heme to iron: the expanding spectrum of heme degrading enzymes used by pathogenic bacteria. Front. Cell. Infect. Microbiol. *8*, 198.

McGrane, R., and Beattie, G.A. (2017). *Pseudomonas syringae* pv. syringae B728a Regulates Multiple Stages of Plant Colonization via the Bacteriophytochrome BphP1. MBio *8*, e01178-17.

Nagata, M., Kaito, C., and Sekimizu, K. (2008). Phosphodiesterase activity of CvfA is required for virulence in Staphylococcus aureus. J. Biol. Chem. *283*, 2176–2184.

Niño-Liu, D.O., Ronald, P.C., and Bogdanove, A.J. (2006). Xanthomonas oryzae pathovars: model pathogens of a model crop. Mol. Plant Pathol. *7*, 303–324.

Noda, T., and Kaku, H. (1999). Growth of Xanthomonas oryzae pv. oryzae in planta and in guttation fluid of rice. Jap. J. Phytopathol. *65*, 9–14.

Oberpichler, I., Rosen, R., Rasouly, A., Vugman, M., Ron, E.Z., and Lamparter, T. (2008). Light affects motility and infectivity of Agrobacterium tumefaciens. Environ. Microbiol. *10*, 2020–2029.

Otero, L.H., Klinke, S., Rinaldi, J., Velázquez-Escobar, F., Mroginski, M.A., Fernández López, M., Malamud, F., Vojnov, A.A., Hildebrandt, P., Goldbaum, F.A., and Bonomi, H.R. (2016). Structure of the full-length bacteriophytochrome from the plant pathogen Xanthomonas campestris provides clues to its long-range signaling mechanism. J. Mol. Biol. *428*, 3702–3720.

Pandey, S.S., Patnana, P.K., Lomada, S.K., Tomar, A., and Chatterjee, S. (2016). Co-regulation of iron metabolism and virulence associated functions by iron and XibR, a novel iron binding transcription factor, in the plant pathogen Xanthomonas. PLoS Pathog. *12*, e1006019.

Pandey, S.S., Patnana, P.K., Rai, R., and Chatterjee, S. (2017). Xanthoferrin, the α-hydroxycarboxylate-type siderophore of Xanthomonas campestris pv. campestris, is required for optimum virulence and growth inside cabbage. Mol. Plant Pathol. *18*, 949–962.

Pandey, S.S., Patnana, P.K., Padhi, Y., and Chatterjee, S. (2018). Low-iron conditions induces the hypersensitive reaction and pathogenicity *hrp* genes expression in *Xanthomonas* and is involved in modulation of hypersensitive response and virulence. Environ. Microbiol. Rep. *10*, 522–531.

Povolotsky, T.L., and Hengge, R. (2012). 'Life-style' control networks in Escherichia coli: signaling by the second messenger c-di-GMP. J. Biotechnol. *160*, 10–16.

Pradhan, B.B., Ranjan, M., and Chatterjee, S. (2012). XadM, a novel adhesin of *Xanthomonas oryzae* pv. *oryzae*, exhibits similarity to Rhs family proteins and is required for optimum attachment, biofilm formation, and virulence. Mol. Plant Microbe Interact. *25*, 1157–1170.

Rai, R., Ranjan, M., Pradhan, B.B., and Chatterjee, S. (2012). Atypical regulation of virulence-associated functions by a diffusible signal factor in Xanthomonas oryzae pv. oryzae. Mol. Plant Microbe Interact. *25*, 789–801.

Rai, R., Javvadi, S., and Chatterjee, S. (2015). Cell-cell signalling promotes ferric iron uptake in Xanthomonas oryzae pv. oryzicola that contribute to its virulence and growth inside rice. Mol. Microbiol. *96*, 708–727.

Ray, S.K., Rajeshwari, R., Sharma, Y., and Sonti, R.V. (2002). A high-molecular-weight outer membrane protein of *Xanthomonas oryzae* pv. *oryzae* exhibits similarity to non-fimbrial adhesins of animal pathogenic bacteria and is required for optimum virulence. Mol. Microbiol. *46*, 637–647.

Römling, U., and Simm, R. (2009). Prevailing concepts of c-di-GMP signaling. Contrib. Microbiol. *16*, 161–181.

Rockwell, N.C., Su, Y.S., and Lagarias, J.C. (2006). Phytochrome structure and signaling mechanisms. Annu. Rev. Plant Biol. *57*, 837–858.

Römling, U., Galperin, M.Y., and Gomelsky, M. (2013). Cyclic di-GMP: the first 25 years of a universal bacterial second messenger. Microbiol. Mol. Biol. Rev. *77*, 1–52.

Ryjenkov, D.A., Tarutina, M., Moskvin, O.V., and Gomelsky, M. (2005). Cyclic diguanylate is a ubiquitous signaling molecule in bacteria: insights into biochemistry of the GGDEF protein domain. J. Bacteriol. *187*, 1792–1798.

Sambrook, J., and Russell, D.W. (2001). Molecular Cloning: A Laboratory Manual. In Cold Spring Harbor Lab, 3rd Ed. (Plainview, NY: Press), p. 413.

Santamaría-Hernando, S., Rodríguez-Herva, J.J., Martínez-García, P.M., Río-Álvarez, I., González-Melendi, P., Zamorano, J., Tapia, C., Rodríguez-Palenzuela, P., and López-Solanilla, E. (2018). Pseudomonas syringae pv. tomato exploits light signals to optimize virulence and colonization of leaves. Environ. Microbiol. *20*, 4261–4280.

Scheiermann, C., Kunisaki, Y., and Frenette, P.S. (2013). Circadian control of the immune system. Nat. Rev. Immunol. *13*, 190–198.

Schirmer, T., and Jenal, U. (2009). Structural and mechanistic determinants of c-di-GMP signalling. Nat. Rev. Microbiol. *7*, 724–735.

Schmitt, M.P. (1997). Utilization of host iron sources by Corynebacterium diphtheriae: identification of a gene whose product is homologous to eukaryotic heme oxygenases and is required for acquisition of iron from heme and hemoglobin. J. Bacteriol. *179*, 838–845.

Sharma, M., and Bhatt, D. (2015). The circadian clock and defence signalling in plants. Mol. Plant Pathol. *16*, 210–218.

Sondermann, H., Shikuma, N.J., and Yildiz, F.H. (2012). You've come a long way: c-di-GMP signaling. Curr. Opin. Microbiol. *15*, 140–146.

Su, J., Zou, X., Huang, L., Bai, T., Liu, S., Yuan, M., Chou, S.H., He, Y.W., Wang, H., and He, J. (2016). DgcA, a diguanylate cyclase from Xanthomonas oryzae pv. oryzae regulates bacterial pathogenicity on rice. Sci. Rep. *6*, 25978.

Swartz, T.E., Tseng, T.S., Frederickson, M.A., Paris, G., Comerci, D.J., Rajashekara, G., Kim, J.G., Mudgett, M.B., Splitter, G.A., Ugalde, R.A., et al. (2007). Blue-light-activated histidine kinases: two-component sensors in bacteria. Science *317*, 1090–1093.

Takala, H., Björling, A., Linna, M., Westenhoff, S., and Ihalainen, J.A. (2015). Light-induced changes in the dimerization interface of bacteriophytochromes. J. Biol. Chem. *290*, 16383–16392.

Tsuchiya, K., Mew, T.W., and Wakimoto, S. (1982). Bacteriological and pathological characteristics of wild types and induced mutants of Xanthomonas campestris pv. oryzae. Phytopathology *72*, 43–46.

Valentini, M., and Filloux, A. (2016). Biofilms and cyclic di-GMP (c-di-GMP) signaling: lessons from Pseudomonas aeruginosa and other bacteria. J. Biol. Chem. *291*, 12547–12555.

van der Horst, M.A., Key, J., and Hellingwerf, K.J. (2007). Photosensing in chemotrophic, non-phototrophic bacteria: let there be light sensing too. Trends Microbiol. *15*, 554–562.

Vierstra, R.D., and Davis, S.J. (2000). Bacteriophytochromes: new tools for understanding phytochrome signal transduction. Semin. Cell Dev. Biol. *11*, 511–521.

Wang, G.Y., Shi, J.L., Ng, G., Battle, S.L., Zhang, C., and Lu, H. (2011). Circadian clock-regulated phosphate transporter PHT4; 1 plays an important role in Arabidopsis defense. Mol. Plant *4*, 516–526.

Wegele, R., Tasler, R., Zeng, Y., Rivera, M., and Frankenberg-Dinkel, N. (2004). The heme oxygenase(s)-phytochrome system of Pseudomonas aeruginosa. J. Biol. Chem. *279*, 45791–45802.

Wu, L., McGrane, R.S., and Beattie, G.A. (2013). Light regulation of swarming motility in Pseudomonas syringae integrates signaling pathways mediated by a bacteriophytochrome and a LOV protein. MBio *4*, e00334-13.

Zarei, S., Taghavi, S.M., Hamzehzarghani, H., Osdaghi, E., and Lamichhane, J.R. (2018). Epiphytic growth of Xanthomonas arboricola and Xanthomonas citri on non-host plants. Plant Pathol. *67*, 660–670.

Zhang, P.J., Broekgaarden, C., Zheng, S.J., Snoeren, T.A., van Loon, J.J., Gols, R., and Dicke, M. (2013). Jasmonate and ethylene signaling mediate whitefly-induced interference with indirect plant defense in Arabidopsis thaliana. New Phytol. *197*, 1291–1299.

STAR★METHODS

KEY RESOURCES TABLE

REAGENT or RESOURCE	SOURCE	IDENTIFIER
Antibodies		
Anti-DDDDK tag antibody	Abcam	Cat#205606
Rabbit anti 6 X His antibody	Abcam	Cat#ab9108; RRID: AB_307016
Goat anti-rabbit HRP-conjugated	Sigma Aldrich	Cat# A9169; RRID: AB_258434
Bacterial Strains		
Xanthomonas oryzae pv. *oryzae*: BXO43 (WT)	Kumar Verma et al., 2018	N/A
X. oryzae pv. *oryzae*:: pHM1	This paper	N/A
X. oryzae pv. *oryzae*: Δ*bphP*	This paper	N/A
X. oryzae pv. *oryzae*: Δ*bphP*(BphP^{+})	This paper	N/A
X. oryzae pv. *oryzae*: Δ*PAS2*	This paper	N/A
X. oryzae pv. *oryzae*: Δ*GAF*	This paper	N/A
X. oryzae pv. *oryzae*: Δ*PHY*	This paper	N/A
X. oryzae pv. *oryzae*: Δ*PAS4*	This paper	N/A
X. oryzae pv. *oryzae*: *XoobphP*$_{C13A}$ carrying alanine substitution for Cys^{13} in *Xoo*BphP	This paper	N/A
X. oryzae pv. *oryzae*: *XoobphP*$_{E131A}$ carrying alanine substitution for Glu^{131} in *Xoo*BphP	This paper	N/A
X. oryzae pv. *oryzae*: Δ*bphP*:: pHM1	This paper	N/A
X. oryzae pv. *oryzae*: Δ*bphP*:: PA3947	This paper	N/A
Escherichia coli: DH5α	Lab collection	N/A
E. coli: BL21(DE3)	Lab collection	N/A
E. coli: BL21(DE3) carrying pRKV41	This paper	N/A
E. coli: BL21(DE3) carrying pRKV42	This paper	N/A
E. coli: BL21(DE3) carrying pRKV43	This paper	N/A
E. coli: BL21(DE3) carrying pRKV44	This paper	N/A
E. coli: BL21(DE3) carrying pRKV45	This paper	N/A
E. coli: BL21(DE3) carrying pRKV46	This paper	N/A
Chemicals, Peptides and Recombinant Proteins		
High-fidelity Phusion *Taq* polymerase	Thermo scientific	Cat# F-530L
Taq DNA polymerase	NEB	Cat# M0320L
Superscript III Reverse Transcriptase	Invitrogen	Cat# 18080044
EcoRI-HF	NEB	Cat# R3101S
HindIII-HF	NEB	Cat# R3104S
BamHI-HF	NEB	Cat# R3136S
*Xba*I	NEB	Cat# R0145
T4 DNA Ligase	NEB	Cat# M0202S
Biliverdin hydrochloride	Sigma	Cat# 30891
Cyclic-di-GMP sodium salt	Sigma	Cat# SML1228
cGMP sodium salt	Biolog	Cat# G001
GMP disodium salt hydrate	Sigma	Cat# G8377
Bis(*p*- nitrophenyl) phosphate sodium salt	Sigma	Cat# N3002
2, 2′- dipyridyl disulfide	Sigma	Cat# 8.41109
Streptonigrin	Sigma	Cat# S1014
*Xoo*BphP	This paper	N/A
*Xoo*BphPΔPAS2	This paper	N/A

(*Continued on next page*)

Continued

REAGENT or RESOURCE	SOURCE	IDENTIFIER
*Xoo*BphPΔGAF	This paper	N/A
*Xoo*BphPΔPHY	This paper	N/A
*Xoo*BphPΔPAS4	This paper	N/A
*Xoo*BphPC13A	This paper	N/A
*Xoo*BphPE131A	This paper	N/A
Critical Commercial Assays		
QIAquick Gel Extraction Kit	QIAGEN	Cat# 28704
QIAGEN Plasmid Midi Kit	QIAGEN	Cat# 12143
DyNAmo ColorFlash SYBR Green qPCR Kit	Thermo scientific	Cat# F-416L
Deposited Data		
Microarray dataset	This paper	Gene Expression Omnibus (https://www.ncbi.nlm.nih.gov/geo/): GSE141343
Experimental Models		
Rice plant Taichung Native-1' (TN-1)	Kumar Verma et al., 2018	N/A
Tomato plant	Pandey et al., 2018	N/A
Oligonucleotides		
All the primers are listed in Table S1	This paper	N/A
Recombinant DNA		
All the primers are listed in Table S2	This paper	N/A

RESOURCE AVAILABLITY

Lead Contact

Further information and requests for resources and reagents should be directed to and will be fulfilled by the Lead Contact, Subhadeep Chatterjee (subhadeep@cdfd.org.in).

Materials Availability

All unique/stable reagents generated in this study are available from the Lead Contact with a completed Materials Transfer Agreement.

Data and Code Availability

The accession number for the microarray data reported in this paper is GEO: GSE141343 and will be available at Gene Expression Omnibus (https://www.ncbi.nlm.nih.gov/geo/).

EXPERIMENTAL MODEL AND SUBJECT DETAILS

Bacterial strains

Xanthomonas oryzae pv. *oryzae* (BXO43) strain was used as the parental strain. *Xoo* parental and mutant strains were grown in rich peptone sucrose agar (PSA) or in PS broth supplemented with appropriate antibiotics (Tsuchiya et al., 1982) at 28°C and 200 rpm (New Brunswick Scientific, Innova 43, Edison, NJ, USA). *Escherichia coli* strains were grown in LB broth supplemented with appropriate antibiotics (detailed information on the *Xoo* and *E. coli* strains used in this study are provided in the Key Resources Table. The concentrations of antibiotics used were as follows: rifampicin (Rif; 50 μg/mL); spectinomycin (Spec; 50 μg/mL); kanamycin (Kan; 50 μg/mL); ampicillin (Amp; 100 μg/mL); gentamycin (Gent; 5 μg/mL); nalidixic acid (Nal; 50 μg/mL).

Bacterial mutant and complemented strain generation

The *XoobphP* (Xoo0292) gene in *Xoo* was deleted utilizing pK18mobSacB system, a suicidal vector, harboring kanamycin resistance gene (kan^R) and *SacB* gene as selection and counter-selection marker respectively, as described earlier (Kumar Verma et al., 2018). The oligonucleotide primers used for constructing the deletion strains are listed in the Key Resources Table. *In frame* deletion mutants of (Δ*PAS2,* Δ*GAF,* Δ*PHY and* Δ*PAS4*) domains of the bacteriophytochrome protein (*Xoo*BphP), were also constructed following the same procedure mentioned above. Complementing strain [(Δ*bphP*($BphP^+$)] was generated by reconstituting the full-length gene (*XoobphP*) into the genomic background of the full-length deletion mutant (Δ*bphP*) by using pK18mobSacB system as described earlier (Kumar Verma et al., 2018). *Xoo* strain showing ectopic expression (Δ*bphP*::PA3947) was constructed incorporating

recombinant pHM1 having a well-characterized phosphodiesterase PA3947, an EAL-containing phosphodiesterase (PDE) encoding gene from *Pseudomonas aeruginosa* PA01 (Deng et al., 2012).

METHOD DETAILS

Molecular biology techniques

Standard genetics and molecular techniques were used for genomic DNA isolation, plasmid isolation, restriction enzyme digestion, ligation, transformation and agarose gel electrophoresis, as described previously (Sambrook and Russell, 2001). High-fidelity Phusion *taq* polymerase (Thermo Fisher Scientific, Waltham, MA, USA), *Taq* DNA polymerase, restriction and ligation enzymes were used according to the manufacturer's instructions. DNA transformations were performed by either heat shock or electroporation. The oligonucleotide primers used in this study are listed in the Key Resources Table. SDS-PAGE, polyacrylamide gel staining and western blot experiments were carried out as described previously (Biswas et al., 2014). All oligonucleotide primers and recombinant DNA clones used in this study are described in detail in the Tables S1 and S2, respectively.

Site directed mutagenesis

Site-directed mutagenesis to introduce the alterations C13A and E131A was done by using mutagenic PCR in a two-step protocol (Deng et al., 2012). In the first round of PCR, two separate reactions were carried out by using the forward and reverse primers shown above together with one of a pair of primers of complementary sequence carrying the desired alteration and the *Xoo* genomic DNA as template (Mutagenic primer sequences are given in Key Resources Table). The products of the first round of PCR were used as templates for a second round of PCR with forward and reverse primers.

Cloning, overexpression and purification of His-tagged XooBphP and its variants

XoobphP gene was amplified using *Xoo* genomic DNA as a template and primers (SCV His6*Xoo*BphP F *EcoR*I and SCV *Xoo*BphP R *Hind*III) and cloned into *EcoR*I and *Hind*III restriction sites of pET28a overexpression vector using a standard protocol (Biswas et al., 2017). Domain deletion variants of *Xoo*BphP (*Xoo*BphPΔPAS2, *Xoo*BphPΔGAF, *Xoo*BphP ΔPHY and *Xoo*BphPΔPAS4) were also cloned into pET28a following similar protocol. Recombinant pET28a vectors (listed in the Key Resources Table) were transformed into *E. coli* BL21(DE3) cells. *Xoo*BphP and its domain deletion and point mutant variants were purified as N-terminal his-tagged variant by Co^{2+}-TALON affinity chromatography following a standard protocol (Biswas et al., 2014). Briefly, exponentially cultivated recombinants of respective variants were exposed to 100 μM IPTG overnight at 18°C and the induced cells were step wisely collected, washed with a 0.9% NaCl solution. The bacterial pellet was resuspended in lysis buffer [20 mM HEPES (pH 7.4), 150 mM NaCl, 10μg/mL PMSF] and disrupted by sonication. The supernatant was passed through Co^{2+}-TALON beads (QIAGEN), followed by extensive washing to remove the contaminants. Finally, his-tagged recombinant proteins were eluted [Elution buffer: 20 mM HEPES (pH 7.4), 150 mM NaCl, 250 mM Imidazole]. Holo proteins were formed by incubating the apo proteins for 1 h at room temperature in the presence of BV (Sigma-Aldrich) followed overnight dialysis against Buffer A [20 mM HEPES (pH 7.4), 300 mM NaCl, 5% glycerol]. Protein concentrations were estimated by the Bradford method (Bradford, 1976).

UV–vis spectroscopy

Holo protein solutions containing 1 mg/ml of *Xoo*BphP or its variants in buffer A [20 mM HEPES (pH 7.4), 300 mM NaCl, 5% glycerol] were taken in a Quartz cuvette and irradiated with a white, blue (470 nm), red (630 nm) or far-red (733 nm) for 10 min (Wu et al., 2013) from Marubeni America Corporation, with plates at a distance under the diodes such that the light intensities were 30, 5, 10, and 0.8 $\mu M\ m^{-2}\ s^{-1}$ for the blue, red, and far-red lights, respectively. Absorption spectra were collected in VAIOSCAN FLASH (Thermo Scientific) multimode microplate reader and plotted using GraphPad PRISM5. The dark states were determined after proteins were kept for dark adaptation (96 h).

Swimming motility assay

Swim plate assay was performed as described previously (Kumar Verma et al., 2018). Different strains of *Xoo* were grown to mid-exponential phase in PS, centrifuged, washed with sterile PBS and normalized to an OD_{600} of 1.0. 5 μL of the normalized suspension was inoculated at the center of semi-solid swim plates (0.1% Agar containing PS medium) and incubated at 28°C static condition for 48 h at white light, dark and red light with intensities same as UV-vis spectroscopy. The motility was quantified by measuring the diameter of swimming motility zone.

Quantitative chemotaxis assay by syringe capillary method

The chemotaxis assay was carried out by the syringe capillary method as described previously (Kumar Verma et al., 2018). Briefly, *Xoo* were grown to mid-exponential phase in PS, centrifuged, and washed with sterile PBS. Capillary tubes (0.45 mm X 13 mm; single-use syringe 1 mL, Dispo Van, Faridabad, Haryana, India) containing various 0.22 μm (Millex-GS, Mumbai, India) filter-sterilized guttation fluid extracted from *Xoo* susceptible rice variety, Taichung Native-1' (TN-1) maintained under high humid conditions in specially built incubation chambers (Kumar Verma et al., 2018), were incubated with cell suspension (in 0.5-mL Eppendorf tubes) of *Xoo* strains at 28°C for 4 h. The content of the capillary was serially dilution plated on PSA for determining the CFU of bacteria

migrated in the capillary. RCR (Relative chemotaxis ratio) was quantified as the number of migrated bacterial cells in the syringe capillary containing the test chemo-attractant to the number of migrated cells in the bacterial syringe capillary containing PBS (pH 7.4) to rule out cells migrated either as a result of bacterial random motility or diffusion.

In planta Virulence assays on rice leaves

Virulence assay was performed by both wound and surface inoculation methods on *Xoo* susceptible rice variety, Taichung Native-1' (TN-1). Rice plants have been maintained under greenhouse condition at 30°C temperature and 60% relative humidity with a daily light period of 12 h. Wound inoculation was performed by the leaf clipping method (Kauffman, 1973). In light-dependent virulence assays, *Xoo* strains were grown to mid-exponential phase in PS and then they were exposed to white light, red light (630 nm) with the same intensities as used in UV-vis spectroscopy and dark adaptation for 4 h. The cells were centrifuged, washed with sterile PBS and normalized to an OD_{600} of 0.6. Sterile surgical scissors dipped in these culture suspensions were used to clip the 40–45-day-old healthy leaf tips. After 2 weeks' post-inoculation, the lesion was quantified by measuring the lesion length. For each strain, at least 20 leaves were inoculated per experiment. To compare the bacterial population in the infected leaves at different days' post-inoculation (dpi), approximately 1-cm pieces right below the lesion were cut by sterile surgical scissors, serially dilution plated and incubated on PS agar plates supplemented with antibiotics (rifampicin, cycloheximide, and cephalexin) at 28°C. Colony forming units (CFU) were counted and documented.

Epiphytic infection was performed by surface inoculation method as described earlier (Kumar Verma et al., 2018). *Xoo* strains were cultivated to mid-exponential phase in PS, centrifuged, washed with sterile PBS (pH 7.4) and normalized to an OD_{600} of 0.6. The healthy rice leaf tips of 30–35-day-old leaves of susceptible variety TN-1 were dipped about 1 cm for 1 min and epiphytic infection efficiency estimated 21 dpi. To determine the epiphytic efficiency after 21 days of post surface inoculation (epiphytic infection), the total number of leaves exhibiting disease lesions were counted and the epiphytic efficiency or the percentage of infection was calculated against the total number of leaves inoculated. To determine the epiphytic entry efficiency after 4 h of epiphytic infection approximately 1-cm pieces right from the leaf tip were cut by sterile surgical scissors, serially dilution plated and incubated on PS agar plates supplemented with antibiotics (rifampicin, cycloheximide, and cephalexin) at 28°C. Colony forming units (CFU) were counted and documented.

Migration of X. oryzae pv. oryzae inside the leaves

The migration assay was performed as described previously with slight modification (Chatterjee and Sonti, 2002). 5 dpi leaves were detached from the plant and surface sterilized in 0.5% sodium hypochlorite solution (Thermo Fisher Scientific, India) followed by repeated washing in 70% ethanol (Commercial Alcohols, Brampton, Canada) and sterile DDW. Leaves were cut into approximately 1-cm pieces opposite of the site of inoculation by sterile surgical scissors and incubated on PS agar plates supplemented with antibiotics (rifampicin, cycloheximide, and cephalexin) at 28°C. Migration was estimated by observing colonies formed after 3-5th day from the bacterial ooze from the cut ends of leaves.

Extracellular Enzyme assay

Extracellular cellulase assay was carried out as described previously (Rai et al., 2012; Kumar Verma et al., 2018) using 0.2% CMC (Sigma-Aldrich, St. Louis) as substrate. Freshly grown bacterial colonies of different *Xoo* strains were spotted on carboxymethyl cellulose (CMC)-PSA plates and incubated for 48 h, followed by Congo red staining (Rai et al., 2012) and washed with 1M NaCl. β-1,4-endoglucanase activity of respective strains was estimated by measuring the degradation halo (halo diameter to colony diameter ratio) produced in CMC-PSA plates.

Separation and quantification of EPS

Extracellular polysaccharide (EPS) was isolated from the cell-free culture supernatant of *Xoo* strains as reported previously (Javvadi et al., 2018). Briefly, 5-6 days cultivated cells were harvested from PSA plates by centrifugation, resuspended in PBS and EPS was precipitated by adding formamide and two volumes of ice-cold acetone followed by incubation at 4°C overnight. Before pelleting cells, 100 μL was aliquoted to perform serial dilution plating for CFUs determination. Next day EPS was centrifuged at 7,969 g for 20 min and the pellet was dried followed by the total carbohydrate content quantification using phenol-sulfuric acid colorimetric method and D-glucose as the standard. Assays were performed in triplicate.

Static biofilm and attachment assay

Biofilm assay was performed as described previously (Rai et al., 2012, Kumar Verma et al., 2018). In brief, different *Xoo* strains were grown overnight in PS broth medium supplemented with the required antibiotics at 28°C and 200 rpm, centrifuged, washed and resuspended in sterile PBS. Approximately, $1x\ 10^9$ cells were transferred into 2 mL of fresh PS medium in 24-well sterile polystyrene culture plates and incubated at 28°C without shaking. After 48 h, the medium was decanted gently, the wells were washed with autoclaved Milli-Q water followed by staining with 0.1% crystal violet. Excess stain was removed by washing and the absorbance of the attached cells dissolved in 90% ethanol was measured at 570 nm.

For attachment assay, cells were cultivated in 24-well polystyrene plates as biofilm assay. After washing the wells, attached cells were resuspended in PBS (pH 7.4) and dilution plated for cell attachment quantification.

Growth assay

Growth assays of different *Xoo* strains were performed according to a standard protocol (Pandey et al., 2016). *Xoo* strains were grown to mid-exponential phase in PS, centrifuged, washed with sterile PBS and normalized to an OD_{600} of 0.6 and 0.1% of these normalized cultures were grown in PS medium, PS medium supplemented with 100 μM 2, 2′- dipyridyl (DP) up to 48 h in 28°c at 200 rpm in a shaker incubator (New Brunswick Scientific, Innova 43, Edison, NJ, USA).

CAS plate assays for siderophore production

The siderophore production assays were performed as described previously (Pandey et al., 2016). Individual colonies of different *Xanthomonas* strains were spotted on peptone sucrose agar (PSA)-chrome azurol sulfonate (CAS) Agar siderophore indicator plates containing 75 μM 2, 2′-dipyridyl. Plates were incubated at 28°C for 48 h. The appearance of yellow halo indicative of secreted siderophore production was estimated by measuring the ratio of halo diameter and colony diameter.

Siderophore estimation by HPLC

Siderophore estimation of the purified vibrioferrin from cell-free culture supernatant of *Xoo* strains by HPLC quantification method was performed as reported previously (Rai et al., 2015; Pandey et al., 2017) with certain modifications. The *Xoo* strains were grown to an OD_{600} of 1.2 in PS broth supplemented with ferrous iron chelator 75 μM 2, 2′- dipyridyl. The bacterial cell cultures were centrifuged and the supernatant was acidified. The acidified supernatant was filtered with 0.22 μm filter (MILLIPORE), then passed through Amberlite XAD-16 resin (Sigma) column and eluted with methanol (Sigma) in fractions. Each fraction was tested for siderophore on the PSA-CAS plates containing 50 μM 2, 2′-bipyridyl. The concentrated siderophore positive fractions were run through Agilent 1100 series HPLC system (Agilent, Santa Clara, CA, USA) and siderophore was estimated comparing with the standard curves generated using a known concentration of a pure standard vibrioferrin (a kind gift provided by Masaki J Fujita, Hokkaido University, Japan).

SNG sensitivity assay

The SNG sensitivity assay was performed to determine intracellular iron levels, as SNG causes cell death by reacting with free ferrous iron to produce superoxide and hydroxyl free radicals as described earlier (Kumar Verma et al., 2018). *Xoo* strains were grown to mid-exponential phase in PS, pelleted, washed with sterile PBS and normalized to an OD_{600} of 1.0. Cultures were serially diluted and then spotted on PSA containing 0.02 μg/mL of SNG (Sigma Aldrich, St. Louis, MO, USA). Plates were then incubated at 28°C for 72 h to observe growth inhibition.

Determination of intracellular iron concentration by ICP-OES

Intracellular iron levels *Xoo* strains were measured by inductively coupled plasma-optical emission spectroscopy (JY 2000 sequential ICP-OES spectrometer, Jobin Yvon, Horiba, France), as described previously (Pandey et al., 2016). The bacteria were cultured in PS, PS plus 50 μM DP or PS plus 50 μM $FeCl_3$/$FeSO_4$ media up to an OD_{600} of 1.2 and cells were harvested by centrifugation, pellets were washed twice with phosphate buffer saline (PBS) to remove EPS, lyophilized and dry weight was measured. Further, the lyophilized cells were dissolved in 30% HNO3 at 80°C for overnight and then diluted 10-fold with sterile Mili Q water. The iron atom content was then measured using ICP-OES. Quantification of iron was performed against an aqueous standard of iron traceable to the NIST (National Institute of Standards and Technology, India).

Iron uptake assay

In-vitro radiolabelled ^{55}Fe uptake assay performed as reported previously (Javvadi et al., 2018) with certain modifications. Bacterial cells were grown in iron-depleted medium (PS plus 100 μM 2, 2′-dipyridyl) for 24 h, washed twice with 50 mM PBS, pH 7.4, resuspended in Chelex-100 (Sigma)-treated PS to an OD_{600} of 1.0 and incubated at 28°C for 5 min. Iron uptake was initiated by addition of 0.5 μM of $^{55}FeCl_3$ of specific activity 10.18 mCi/mg (American radiolabelled chemicals, Inc., St. Louis, USA). The stock solution was diluted ten times with either water for the $^{55}Fe^{3+}$ uptake studies or with 1M sodium ascorbate (to convert $^{55}Fe^{3+}$ into $^{55}Fe^{2+}$) for $^{55}Fe^{2+}$ uptake studies. At different time points, 200 μL of the cell suspension was layered onto di-butyl phthalate–di-octyl phthalate (1:1) mixture and centrifuged at 13000 rpm for 1 min to stop the uptake during the 15-min time-course of the experiment. The aqueous layer was aspirated, and the pellet was resuspended in 100 μL of 1% (v/v) Triton X-100, the suspension was placed in 5 ml of scintillation cocktail and counted in the ^{3}H channel of scintillation counter (Tri-Carb 2910 TR Liquid Scintillation Analyzer; Perkin Elmer, USA). Assays were performed in triplicate.

Intrinsic tryptophan fluorescence

The intrinsic tryptophan fluorescence spectra (λ_{ex} = 280nm and λ_{em} = 290–400 nm) of *Xoo*BphP in absence and presence of increasing concentration of $FeCl_3$ (0-100 μM) and $FeSO_4$ (0-100 μM) was recorded using Hitachi F-3000 spectrofluorometer as reported previously (Biswas et al., 2019). Protein concentrations used in each experiment was 5 μM. Similar experiment was performed with Bovine serum albumin (BSA) in absence and presence of $FeCl_3$. (bandwidth of 5 nm for both excitation and emission). The observed fluorescence intensities were corrected by subtracting the corresponding buffer fluorescence. The equilibrium dissociation constant (K_D) was determined by nonlinear fitting of the fluorescence data to the "one-site specific binding" Equation 1 using GraphPad Prism (GraphPad Software Inc.) as described earlier (Jana et al., 2012).

$$Y = (Bmax[X])/(KD[X]) \quad \text{[Equation 1]}$$

where Y indicates the extent of fluorescence quenched at any $FeCl_3$ concentration ([X]), which was determined by subtracting the fluorescence in the presence of $FeCl_3$ from the fluorescence in the absence of $FeCl_3$. B_{max} (i.e., maximal fluorescence quenched upon saturation of protein with $FeCl_3$).

PDE activity assay

PDE activity of *Xoo*BphP and its variants were determined using bis *p*NPP following a standard protocol (Chen et al., 2004; Nagata et al., 2008). The protein was incubated with increasing concentration of bis *p*NPP (0-10 mM) at 37°C for 60 min in reaction buffer (0.1 M Tris HCL, pH 8.5 and 1 mM $MnCl_2$). The reaction yielded *p*-nitrophenol, which became an intense yellow soluble product under alkaline conditions and was measured at 405 nm on a spectrophotometer (Spectra Max M5, Molecular Devices). The kinetic parameters were deduced by fitting the initial velocities (V_0) at various substrate concentrations to the Michaelis–Menten equation (*E2*) using the Prism software (GraphPad Inc.). Assays were performed in triplicate.

Cyclic nucleotide phosphodiesterase activity by HPLC

High-pressure liquid chromatography analysis to separate nucleotides was done as described previously (Deng et al., 2012). Phosphodiesterase reactions were undertaken in 20 μL reactions containing 2.5 μM purified *Xoo*BphP variants, 0.1M Tris-HCl (pH 8.5), 0.5 mM c-di-GMP or cGMP and 1 mM $MnCl_2$. Reactions were incubated at 37°C for 90 min, stopped by heating at 75°C for 5 min followed by a centrifugation. The analysis of supernatant was performed by reverse-phase HPLC on a SHIMADZU LC-2030C 3D Prominence-i series HPLC system. Samples of 5 μL were injected into a Shim-Pack GIST 5 μm C-18 column and fractionated by using 15% (vol/vol) acetonitrile/100% 10 mM ammonium acetate buffer (pH 6.3) under isocratic condition at a flow rate of 0.3 ml/min. Nucleotides were detected at a wavelength of 252 nm. The nucleotides were identified comparing the retention time of the different standard nucleotides run in the same column and the identity of the nucleotides were further confirmed by mass spectrometry.

Extraction and quantification of intracellular c-di-GMP

Nucleotides were extracted using a protocol as described previously (Su et al., 2016). Briefly, after cultivating at 28°C, 200 r min−1 for OD_{600} (1.2-1.5) in 100 mL PS, 0.2% formaldehyde (Sigma) was added to stop the cellular activity, and cells were centrifuged at 4°C for 20 min at 6000 r min−1, and further washed twice with fresh PBS (pH7.4). Next, cells were resuspended by vigorous pipetting in 10 mL extraction buffer [40% methanol, 40% acetonitrile, 0.2 N formic acid and 10% nuclease-free water] and aliquoted in 1 mL in each 2 mL Eppendorf tube, followed by 45-60 min incubation on ice, then 45-60 min incubation at 99°C in Thermomixer. Put some weight on the lid to avoid sample leakage. After cooling down to RT, the sample was centrifuged at 14000 r min−1 for 30 min. The supernatant was kept at −20°C and/or vacuum dried. Next, nucleotide extracts were resuspended in Milli-Q at RT and concentrated by vacuum drying. Next, samples were analyzed by liquid chromatography-tandem mass spectrometry (LC-MS/MS) with a Thermo SCIENTIFIC Q-Exactive HF mass spectrum system. The intracellular c-di-GMP level was presented as nmol/10^7cells.

Hypersensitive response assay

In planta hypersensitive response assay was performed as reported previously (Hauck et al., 2003). *Xoo* cultures were grown up to mid-exponential phase in PS, pelleted, washed with sterile MQ and normalized to an OD*600* of 0.6. The fresh and healthy leaves of 25-30 days old tomato S-22 cultivar (acts as non-host for *Xanthomonas oryzae* pv. *oryzae*) were administered with bacterial culture suspensions and PBS was used as control. Plants were incubated in green house with minimum and maximum temperature of 26 and 28°C, respectively and relative humidity of 65%. Pictures of the leaves infiltrated with different strains were taken after 16-20 hr of infiltration for visualizing the extent of HR-like symptoms in tomato.

Cell fractionation

*Xoo*BphP localization study was performed as reported (Ray et al., 2002). Bacterial cultures grown in Peptone Sucrose broth were pelleted and resuspended in buffer containing 5 mM Tris-Cl (pH 8.0), 0.375 M sucrose, 1 mM EDTA and 30 μg/ml lysozyme. The cell pellet was sonicated and centrifuged at 5000 rpm for 10 min. The supernatant was centrifuged repetitively at 6000 rpm for 8 min until unlysed cells were removed. The supernatant was centrifuged at 90,000 rpm for 2 h in ultracentrifuge. The pellets were resuspended in Triton X-100 buffer containing 10 mM Tris-Cl (pH 8.0), 1% Triton X-100 and 5 mM $MgCl_2$ and incubated for 30 min at RT, followed by ultracentrifugation at 70,000 rpm for 30 min. The supernatant was retained as the inner membrane fraction and the pellet was resuspended in buffer containing 50 mM Tris-Cl (pH 8.0), 10 mM EDTA and 1% Triton X-100 and incubated at RT for 30 min followed by centrifugation at 10,000 rpm for 1 h. The supernatant was collected as outer membrane fraction. Protein normalized samples from all the fractions were loaded on 12.5% SDS-PAGE and stained with Coomassie brilliant blue to recheck the protein normalization and accordingly the volumes were corroborated based on the observation of the band intensities.

Expression analysis by qRT PCR

For expression analysis by qRT PCR, the Trizol (Invitrogen, CA, USA) method was used according to the manufacturer's instructions. The *Xoo* strains were grown in the PS medium with appropriate antibiotics at 28°C, and illuminated under Red light with the intensity used in UV-Vis spectroscopy for 4 h. Then, cells were harvested at mid logarithmic phase by centrifugation at 8000 × g for 20 min at 4°C. Total RNA was isolated using the Trizol (Invitrogen, St. Louis, USA) method as suggested in the manufacturer's protocol and dissolved in 350–40 μ l RNase-free water. cDNA synthesis and Illumina Sequencing were performed as described (Su et al., 2016). Real-time qRT-PCR was performed in a 7500 Real-time PCR system (Applied Biosystems, Foster City, CA 94404. USA) and analyzed by SDS relative quantification software (Applied Biosystems) as described previously (Pandey et al., 2016). Relative quantification of the expression of certain *Xoo*BphP regulated genes in wild-type *Xoo* strain by real-time qRT-PCR were performed following the same procedure under dark and white light exposure. The primers used for real-time qRT-PCR are listed in Key Resources Table.

Gene expression profiling using Agilent microarray platform

The 15K array comprised of a total number of 15,744 features including 15,208 probes and 536 Agilent controls. All the oligonucleotides designed and synthesized *in situ* as per the standard algorithms and methodologies used by Agilent Technology for 60-mer oligonucleotide DNA microarray. Out of 4125 transcripts, 4119 probes were designed from NCBI transcript sequences with an average of 1 probe per sequence.

Blast was performed against the respective sequence database to check the specificity of the probes. Finally, 4119 probes were designed for NCBI transcript sequences and specific probes were replicated to fill the blank spots. The microarray data discussed in this manuscript have deposited in the NCBI Gene Expression Omnibus (GEO) under the GEO series accession number GSE141343.

QUANTIFICATION AND STATISTICAL ANALYSIS

All quantitative experiments were performed in triplicate and average with the standard error of the mean (SEM) was mentioned in the corresponding figure legends. The data are presented as mean ± SD. Student's t test was performed for statistical analysis and respective statistical parameters such as the value of n and the significance levels (*$p < 0.05$, **$p < 0.01$, and ***$p < 0.001$) are mentioned in the figure legends.